Volume 10
Number 39
21 October 2022
Pages 14353–14780

Journal of Materials Chemistry C

Materials for optical, magnetic and electronic devices

rsc.li/materials-c

ISSN 2050-7526

ROYAL SOCIETY OF CHEMISTRY

PAPER

Ke-Qing Zhao, Bertrand Donnio *et al.*

Synthesis, self-assembly and optical properties of some rigid π-bridged triphenylene dimers

Journal of Materials Chemistry C

ROYAL SOCIETY OF CHEMISTRY

PAPER

View Article Online
View Journal | View Issue

Cite this: J. Mater. Chem. C, 2022, 10, 14453

Synthesis, self-assembly and optical properties of some rigid π-bridged triphenylene dimers†

Hang Lin,[a] Ke-Xiao Zhao,[a] Min Jing,[a] Xiu-Hai Long,[a] Ke-Qing Zhao, *[a] Ping Hu,[a] Bi-Qin Wang,[a] Peng Lei,[b] Qing-Dao Zeng [b] and Bertrand Donnio *[c]

The synthesis of an exclusive family of liquid-crystalline dimers consisting of two protomesogenic triphenylene moieties connected *via* a rigid, π-conjugated bridge, and the study of their mesomorphous, gel self-assembly and optical properties as a function of the nature of the bridge are reported. Various triphenylene bridged dimers were successfully prepared by either palladium-catalyzed Suzuki–Miyaura cross-coupling between pentakis(alkoxy)triphenylene nonaflates and various commercially accessible aryldiboronic acids (as bridges) or by $FeCl_3$-promoted Scholl oxidative homo-coupling of thiophene/thienothiophene/furan-containing pentakis(alkoxy)triphenylene derivatives. All linear dimers are mesomorphous, and self-organize into large multi-columnar rectangular superlattices, with columnar pairs arranged according to a chevron-like pattern, as deduced from SWAXS and supported by STM. At high temperature, most compounds also display a nematic columnar mesophase (N_{Col}), easily recognized by characteristic optical textures. The transition temperature and mesophase ranges show a high dependency on the bridge nature and, to a lesser extent, on the chain-lengths around the triphenylene moieties. The sole kinked bridged-dimeric homolog of this series exhibits a single, room-temperature hexagonal mesophase (Col_{hex}), as do the monofunctionalized triphenylene precursors, whereas the dimeric triphenylene with no bridge is not mesomorphous. UV-visible absorption and fluorescence emission spectra were measured in both solvents and thin films. The π-conjugated bridged-dimers exhibit emission spanning from 400–700 nm, thus covering the full visible-light range, whose emission maxima are obviously influenced by the chemical nature of the bridge. Furthermore, fluorescence quantum yields as high as 64% were measured for some of them. DFT theoretical computing calculations fully support the experimental measurements. Most dimers also form gels in cyclohexane and emit blue-to-orange light when irradiated by UV light; the corresponding xerogels revealed that their gelation ability results from the 3D morphology of entangled ultra-long and thin microfibers. The facile synthesis of these unique, multifunctional rigid discotic dimers, their rich mesomorphism, strong gelation ability and fine-tuned photophysical properties make these materials very attractive for the active field of organic electronics.

Received 10th June 2022,
Accepted 1st September 2022

DOI: 10.1039/d2tc02441a

rsc.li/materials-c

Introduction

The active search for new π-conjugated polycyclic aromatic hydrocarbons (PAHs) able to meet the insatiable demand and numerous requirements for their implementation in organic electroluminescent devices (OLEDs), organic photovoltaics (OPVs) and organic field-effect transistors (OFETs) has resulted in significant progress in synthetic methodologies, molecular design and, none the least, molecular diversity.[1–3] For the synthesis of PAHs, transition metal-catalyzed Suzuki–Miyaura cross-coupling[4] and intra-/inter-molecular $FeCl_3$-catalyzed Scholl oxidative cyclodehydrogenation[5–11] are among the most used chemical methods. The latter chemical reactions are also of prime importance as they are not only cost-effective and robust synthetic routes, but also possess environmentally friendly characteristics

[a] College of Chemistry and Materials Science, Sichuan Normal University, Chengdu 610066, China. E-mail: kqzhao@sicnu.edu.cn
[b] Key Laboratory of Standardization and Measurement for Nanotechnology, Centre for Excellence in Nanoscience, National Centre for Nanoscience and Technology (NCNST), Beijing 100190, China
[c] Institut de Physique et Chimie des Matériaux de Strasbourg (IPCMS), CNRS-Université de Strasbourg (UMR7504), Strasbourg, 67034, France. E-mail: bertrand.donnio@ipcms.unistra.fr

† Electronic supplementary information (ESI) available: Materials, experimental and synthetic procedures, ^1H, ^{13}C, and ^{19}F NMR, HRMS, UV-vis and photoluminescence spectra, SEM images of xerogels, DFT calculations, TGA curves, POM photos, DSC curves, S/WAXS patterns, STM images, and model variations (111 pages). See DOI: https://doi.org/10.1039/d2tc02441a

and produce small quantities of toxic wastes with recycling possibilities, features that are widely sought after for the sustainable development and carbon footprint reduction of the next generation of organic optoelectronic materials.

The combination of electronic (photophysical and semiconducting) and anisotropic fluid properties within single compounds has also attracted much attention in these advanced fields of research too.[12–14] Liquid crystalline materials possessing π-conjugated polycyclic aromatic cores and peripheral flexible aliphatic chains to improve solubility in organic solvents and promote their spontaneous self-organization into ordered self-healing mesophases further are interesting assets for their potential integration into various optoelectronic-based applications. Their use also permits substantial cost reduction in device fabrication, by, for instance, ink-jet printing or coating existing techniques. π-Extended conjugated discotic liquid crystals (π-DLCs)[15–18] spontaneously self-organize into supramolecular columns promoted by π–π stacking of their polycyclic cores, and these columns further self-assemble into various long-range order nanostructures, *i.e.*, 1D lamello-columnar (LamCol), 2D columnar hexagonal/rectangular (Col_{hex}/Col_{rec}), or 3D helicoidal columnar[19–24] mesophases, propitious to the creation of potentially soft, unidimensional molecular pathways for the transport of electrons and holes.

The relationship between structures and property functions is one of the central topics in materials science to improve systems, but our predictive ability still remains elusive and challenging, hence a systematic exploration of molecular diversity is important. Although the emergence of liquid crystalline phases is quite easily guaranteed by adapted molecular design, some specific geometrical considerations and the association of various molecular species between them make it difficult to predict the types of organizations, as well as their stability and resilience towards thermal/optical/chemical stresses or the characteristics of their intrinsic physical properties.[25] By using the versatile synthetic methods mentioned earlier, a great diversity of π-conjugated heterocyclic molecules has thus emerged, with molecules having cross-,[26–31] board-[32–34] and butterfly-like[35,36] shapes, integrating various types of electroactive molecular units within their structure such as fluorene,[36] fluorenone,[36–38] carbazole,[36] benzothienobenzothiophene,[39,40] or other fused-thiophene[41–50] building blocks. These systems show, as expected by design, mainly columnar mesophases with high thermal stability, as well as, depending on their intrinsic molecular structure, interesting photoluminescence, solvent gelation ability and/or charge carrier mobilities, of relevance for electronics-based applications.

In our search for the development of new and highly-functional molecular systems efficiently synthesized from simple and accessible basic components, we report on an exclusive library of dimeric disk-like mesogenic molecules consisting of two triphenylene moieties connected together by a conjugated, rigid molecular bridge, the liquid crystalline properties being conferred by the two triphenylene units. Surprisingly, only a few of such rigid systems have been reported so far,[51–58] despite both fundamental and practical interests, such as for instance the possibility of numerous chemical alterations of the bridge to tune the physical properties precisely, or the induction of new types of columnar-like and nematic mesophases due to the specific constraints imposed by the inflexible bridge, of particular interest for some of the targeted applications mentioned above. In this work, using a diverse collection of small molecules, several new π-bridged discotic dimers (Scheme 1) were synthesized in good-to-high yields and good purity either by Suzuki–Miyaura cross-coupling of lipophilic monononaflate triphenylenes with appropriate aryl-bisboronic acids (bithiophene-, phenylene-, biphenylene-, thienothiophene- and benzodithiophene-bisboronic acids, respectively, Scheme 1), or by Scholl oxidative homo-coupling of thiophene-/thienothiophene-/furan-monosubstituted triphenylene derivatives (**M1**–**M5**, Scheme 1) to yield bithiophene-, bifuran- and bithienothiophene-bridged triphenylene dimers, respectively. One dimer with no bridge (**Tp^{6}Tp^6**, Scheme 1) was also synthesized to demonstrate the importance of the bridge in the induction of mesophases. In addition, two other, non-symmetrical σ-bridged dimeric compounds (**Tp^{6}T^6** and **Tp^{6}Dt^6**, Scheme 1) were also synthesized by the versatile annulative π-extension (APEX) reaction from some of the monomeric precursors.[59,60] These σ-bridged dimers were found to self-organize into Col_{rec} whereas all the linear π-dimers showed N_{Col} and multi-columnar mesophases with superlattices. Some of the compounds also displayed gelation behavior and interesting optical properties.

Results and discussion

Molecular designing, synthesis and characterization

Lipophilic triphenylene derivatives are workhorses of DLCs,[61–64] and they display outstanding self-organizational behaviors and semi-conductive properties, which can be modulated by the nature of the peripheral substitution.[62–64] The chemistry of functionalized triphenylene derivatives bearing various peripheral molecular moieties, *i.e.* polar (–CN, –SCN, –NC, $–NO_2$, $–CO_2H$, $–NH_2$, N_3, Aryl, ...), halide and hydroxyl groups,[65–69] has been widely explored and well developed to yield appealing functional building blocks for the construction of more complex molecules, dendrimers, polymers, coordination metal complexes, *etc.*[65–69] The corresponding mesogenic triphenylene dimers and oligomers[69–72] connected together by flexible aliphatic spacers tend to exhibit mainly Col_{hex} mesophases, which is explained by the strong decoupling between the discotic units. In contrast, the less-reported rigid discotic dimers, when the two discrete discotic units are directly and physically bonded, and thus interdependent on each other, seem to preferentially dispense different types of mesophases, including also the elusive nematic mesophases (N_D or N_{Col}), due to some strong geometrical and conformational constraints.[53,55] Some of the latter systems have in fact proven to be valuable and have been commercially applied as optical films for widening the view-angle of liquid crystal displays.[64,73] Triphenylene-based dimers, oligomers and polymers containing electron-active aromatic cores, such as thiophene, thienothiophene, dibenzothiophene, and furan moieties, are also

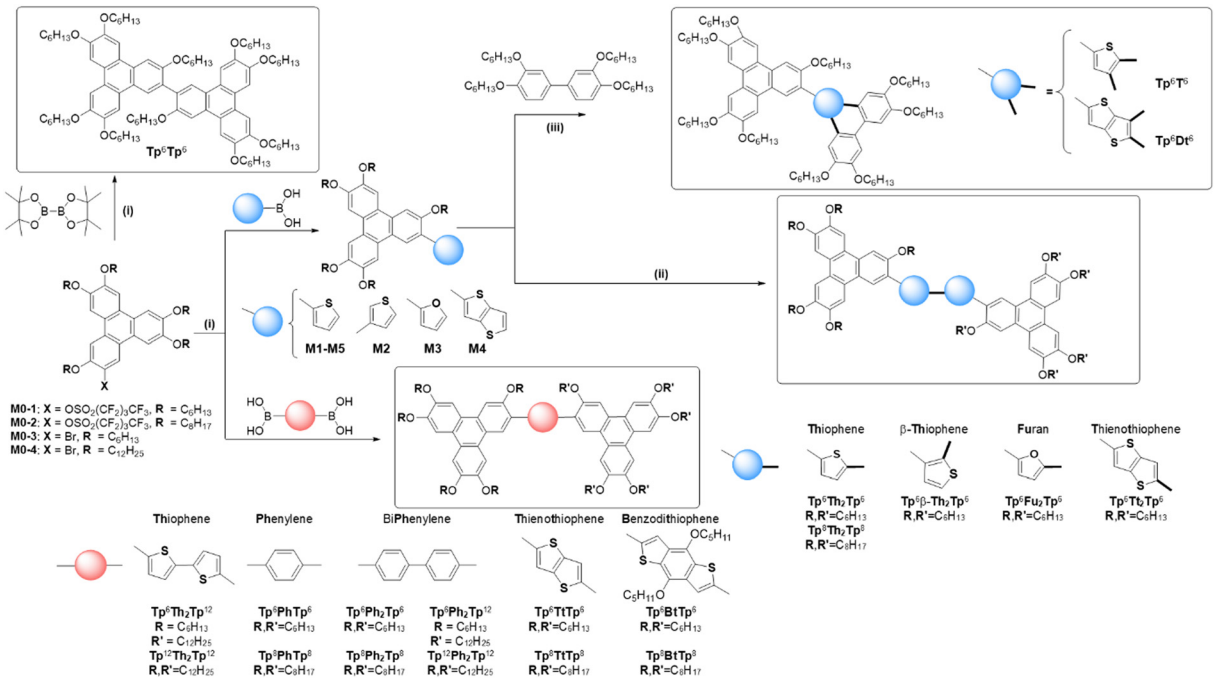

Scheme 1 General synthetic scheme and nomenclature of the various monomeric and dimeric compounds (displayed in the frames): (i) Suzuki coupling; (ii) Scholl oxidative cyclodehydrogenation; and (iii) annulative π-extension (APEX) reactions. Nomenclature: $\mathbf{Tp^{i,j}\text{-}\pi\text{-}Tp^{i,j}}$, where $\mathbf{Tp^{i,j}}$ is the triphenylene moiety substituted by 5 alkoxy chains, OC_nH_{2n+1}, of length $n = i$ and/or j, with i, j = 6, 8, 12, and **π** for the rigid, conjugated bridge: **π** = **Th**, $\mathbf{Th_2}$ for (bi)thiophene-, **Fu**, $\mathbf{Fu_2}$ for (bi)furan-, **Tt**, $\mathbf{Tt_2}$ for (bi)thienothiophene-, **Ph**, $\mathbf{Ph_2}$ for (bi)phenylene-, and **Bt** for benzodithiophene-based bridge.

expected to show interesting supramolecular architectures and superior optical and electrical properties due to the synergy between the different molecular species.

Here, aryl-connected lipophilic triphenylenes (*i.e.* 2-aryl-3,6,7,10,11-pentakis(alkoxy)-triphenylenes, **M1–M5**, Scheme 1 and Scheme S5, ESI†) were designed and used as the main precursors for the synthesis of several novel π-bridged and σ-bonded discotic dimers (Scheme 1). The first set of symmetrical π-bridged dimers was thus obtained by the Scholl oxidative homo-coupling cyclodehydrogenation reaction of thiophene-/thienothiophene-/furan-substituted triphenylene derivatives (Scheme 1 and Scheme S8, S9, ESI†), whereas, another set of dimers, both symmetrical and non-symmetrical, was prepared by the Suzuki–Miyaura cross-coupling reaction (Scheme 1 and Scheme S10, S13, ESI†) between the appropriate aryldiboronic acids and triphenylene nonaflate or bromo derivatives, respectively (**M0–1, M0–2**, Scheme S3, and **M0–3, M0–4**, Scheme S4, ESI†). As for the σ-bonded dimers, they were obtained by the thiophene-biphenyl annulative π-extension (APEX) reaction (Scheme 1 and Scheme S6, S7, ESI†).

The key precursors of **M0–1** and **M0–2**, *i.e.* 2-hydroxy-3,6,7,10,11-pentakis(alkoxy)-triphenylenes, were synthesized as previously reported by the one-pot $FeCl_3$ oxidation of the corresponding 1,2-di(alkoxy)phenylene.[74] Triphenylene triflates were previously successfully applied in the Suzuki–Miyaura cross-coupling reaction for the synthesis of aryl-triphenylenes and triphenylene-fluorene-triphenylene discotic triads.[55,75] However, considering the availability and high cost of the reagents, triphenylene nonaflates[76] were synthesized to replace the triflates and used for the synthesis of the above-mentioned aryl-triphenylenes (Scheme 1). The Suzuki–Miyaura cross-coupling reaction between these triphenylene nonaflates (**M0–1**, **M0–2**) and commercially available or synthesized arylboronic acids produced the five 2-aryl-triphenylenes bearing 2-thiophenyl (**M1**/**M5**), 3-thiophenyl (**M2**), 2-furyl (**M3**), and 2-thieno[3,2-*b*]thiophene (**M4**) moieties, respectively, in high yields of *ca.* 90% (Scheme 1).

Oxidative homo-coupling of these electron-rich triphenylenes (Scheme 1 and Scheme S8, S9, ESI†) gave the corresponding symmetric discotic bridged dimers in good yields ($\mathbf{Tp^6Th_2Tp^6}$ (76%), $\mathbf{Tp^6\beta\text{-}Th_2Tp^6}$ (64%), $\mathbf{Tp^6Fu_2Tp^6}$ (67%), $\mathbf{Tp^6Tt_2Tp^6}$ (71%), and $\mathbf{Tp^8Th_2Tp^8}$ (73%)). For the 2-substituted thiophene (**M1**/**M5**), the 5-position is the most electron-rich and active, and thus, $FeCl_3$ oxidation resulted in the linear, symmetric dimers ($\mathbf{Tp^6Th_2Tp^6}$ and $\mathbf{Tp^8Th_2Tp^8}$). Similarly for 2-substituted furan **M3** and thieno[3,2-*b*]thiophene **M4**, the reaction patterns are the same, and the corresponding π-extended linear dimers $\mathbf{Tp^6Fu_2Tp^6}$ and $\mathbf{Tp^6Tt_2Tp^6}$ were thus also easily obtained. For the 3-substituted thiophene **M2**, however, the reaction pattern is different: the oxidative homo-coupling occurred at the 2-position, yielding only $\mathbf{Tp^6\beta\text{-}Th_2Tp^6}$, and did not occur in the less bulky 5-position; thus other isomers were not produced. It is demonstrated here that the Scholl reaction is electronically-determined but not sterically-driven. Furthermore, dimer $\mathbf{Tp^6\beta\text{-}Th_2Tp^6}$, with a head-to-head coupling product, was the only product isolated, with the complete absence of head-to-tail or tail-to-tail coupled isomers.

In order to demonstrate the great versatility of the Scholl reaction, 2 unsymmetrical σ-bonded discotic-like dimers were

also synthesized by oxidative hetero-cross-coupling (annulated π-extension, APEX) between TP-2-thiophene (**M1**) and TP-2-thieno[3,2-*b*]thiophene (**M4**) and 3,3′,4,4′-tetra(alkoxy)biphenyl, respectively. Indeed, $FeCl_3$-promoted oxidation of 1,2-di(alkoxy)-benzene easily produces symmetrical 2,3,6,7,10,11-hexakis-(alkoxy)-triphenylene in high yields,[77,78] and the cross-coupling of electron-rich tetra(*n*-alkoxy)biphenyl with *o*-di(*m*-alkoxy)-benzene lends the corresponding unsymmetrical triphenylenes (with $n \neq m$).[79] Similarly, thiophene and thienothiophene, as electron-rich arenes, cross-coupled with tetra(alkoxy)biphenyl yield in one step π-extensive thiophene-fused heteroarenes.[39,49] To further extend this reaction, we successfully applied the $FeCl_3$-mediated cross-coupling oxidation of **M1**/**M4** with electron-rich tetra(alkoxy)biphenyl to yield two additional unsymmetrical σ-bonded discotic liquid crystals, **Tp^{6}T^6** and **Tp^{6}Dt^6** (Scheme 1 and Scheme S6, S7, ESI†), isolated in yields of 24 and 64%, respectively, by modifying the addition of **M1**/**M4** to the mixed solution of excess biphenyl and $FeCl_3$ in CH_2Cl_2. The cross-coupling products of unsymmetrical discotic dimers **Tp^{6}T^6**/**Tp^{6}Dt^6**, as well as their homo-coupling symmetrical products **Tp^{6}Th$_2$Tp^6**/**Tp^{6}Tt$_2$Tp^6**, were collected and separated by silica column chromatography. It was noted that **Tp^{6}T^6** was synthesized in much lower yields than **Tp^{6}Dt^6**. **M4**, with a thieno[3,2-*b*]thiophene unit and a larger π-system, is effectively π-conjugated with the triphenylene core; the effective conjugation can inhibit free rotation of thieno[3,2-*b*]thiophene block, which is advantageous to the approach of tetra(hexyloxy)biphenyl for annulation. While the thiophene ring in **M1** is smaller and less π-conjugated with the triphenylene core and more freely to rotate, the approach of tetra(hexyloxy)biphenyl is more difficult and consequently the annulative reaction is less efficient. The other explanation for this result is that the **M1** homo-coupling occurs at a faster rate than cross-coupling; while on the contrary, cross-coupling is faster than homo-coupling for **M4**. It can be anticipated that, in the future, various types of thiophene-containing intermediates as well as electron-rich furan and pyrrole derivatives can be synthesized by this one-step, effective cross-coupling (oxidative APEX reaction)[59,60] for the construction of original organic semiconductors.

The Suzuki–Miyaura cross-coupling was applied for the synthesis of eight other symmetrical π-bridged triphenylene dimers (Scheme 1 and Scheme S10, ESI†): triphenylene nonaflates coupled with the two commercial aryldiboronic acids produced dimers in good yield, *i.e.* **Tp^{6,8}PhTp^{6,8}** (80 and 72%) and **Tp^{6,8}Ph$_2$Tp^{6,8}** (78 and 72%), whilst coupled with the two synthesized aryldiboronic acids yielded dimers **Tp^{6,8}TtTp^{6,8}** (68 and 67%) and **Tp^{6,8}BtTp^{6,8}** (64 and 60%) in good-to-moderate yields. To complete this series, additional non-symmetrical derivatives with a biphenyl and bithiophene bridge were prepared by reacting 4,4'-biphenyldiboronic acid or 5,5′-bis-(4,4,5,5-tetramethyl-1,3,2-dioxaborolan-2-yl)-2,2′-bithiophene, respectively, with a mixture of two 2-bromo-3,6,7,10,11-pentakis(alkoxy)-triphenylene derivatives bearing alkoxy chains with different lengths (**M0–3** and **M0–4**) in the ratio of 1 : 1.1 : 1.1 (Scheme S4, ESI†). For the preparation of **Tp^{6}Ph$_2$Tp^{12}** (Scheme S11, ESI†), **M0–4** was mixed first with 4,4'-biphenyldiboronic acid, and then, after 6 hours and cooling, the other monomer **M0–3** was added to the mixture, and allowed to react for 12 hours. For the synthesis of **Tp^{6}Th$_2$Tp^{12}** (Scheme S12, ESI†), both triphenylene monomers **M0–3** and **M0–4** were mixed in an equimolar ratio at the beginning of the procedure with 5,5′-bis(4,4,5,5-tetramethyl-1,3,2-dioxaborolan-2-yl)-2,2′-bithiophene, and allowed to react together for 24 hours. In each case, the main compounds formed (with same or mixed chain periphery) could be easily separated by chromatography techniques: the non-symmetrical systems (**Tp^{6}Ph$_2$Tp^{12}**and **Tp^{6}Th$_2$Tp^{12}**) and the symmetrical ones (**Tp^{12}Ph$_2$Tp^{12}** and **Tp^{12}Th$_2$Tp^{12}**, along with the other two homologous compounds with hexyloxy chains) were isolated in overall yields of ca 20–30% each.

Finally, a bitriphenylene derivative with no bridge, **Tp^{6}Tp^6**, as the test compound, was also easily prepared by the direct Suzuki coupling between 2-bromo-3,6,7,10,11-pentakis(hexyloxy)-triphenylene and commercial bis(pinacolato)diboron in 71% yield (Scheme 1 and Scheme S13, ESI†).[80]

The complete synthetic details are reported in the experimental section of the ESI.† All the compounds were fully characterized by ^{1}H/^{13}C/^{19}F NMR and elemental analysis, and the final compounds by additional HRMS (See ESI,† Fig. S1–S49).

Thermal behavior and mesomorphism

The thermal and mesomorphic behaviors of the discotic dimers and their aryl-containing triphenylene precursors were studied by polarized optical microscopy (POM) and thermal analyses (differential scanning calorimetry – DSC, and thermal gravimetric analysis – TGA), and the structure of the mesophases by variable temperature small- and wide-angle X-ray scattering (SWAXS). The POM images (Fig. S61, ESI†), TGA (Fig. S62, S63 and Table S7, ESI†) and DSC (Fig. S64–S66 and Table S8, ESI†) curves and the corresponding tables, as well as the SWAXS data (Fig. S67–S70 and Tables S9–S13, ESI†) are available in the ESI.†

The triphenylene structure is one of the simplest and most studied basic polyaromatic systems in discoid liquid crystals.[12,61] Due to its flat and nearly perfect circular shape, and once appropriately substituted in the six lateral positions (*e.g.* 2,3,6,7,10,11-hexasubstitution) by alkyl/alkoxy/ethylene glycol/perfluorinated chains, triphenylene-containing compounds[12,61] show a natural tendency to stack into cylindrical columns with a short stacking distance of *ca.* 3.5 Å (h_{TP}, see below) and to then self-organize mainly into hexagonal columnar mesophases (Col_{hex}), with the chains homogeneously distributed around the piles. The archetypical *n*-alkoxy-chain compounds, included here as reference for comparison, show a columnar hexagonal mesophase, though over a rather narrow temperature range (*e.g.* n = 6, Iso 98 Col_{hex} 53 °C Cr; n = 8, Iso 84 Col_{hex} 46 °C Cr).[81]

In this work, several σ- and π-bridged dimers were thus synthesized from the monosubstituted triphenylene monomers. Two sets of compounds were obtained by the Scholl reaction: i) the unsymmetrical σ-bonded dimers, **Tp^{6}T^6** and **Tp^{6}Dt^6**, by oxidative hetero-cross-coupling of **M1** and **M4**,

respectively, with the electron-rich (tetrahexyloxy)biphenyl, and ii) the symmetrical dimers **Tp^{6}Th$_2$Tp^6**, **Tp^{6}β-Th$_2$Tp^6**, **Tp^{6}Fu$_2$Tp^6**, **Tp^{6}Tt$_2$Tp^6**, and **Tp^{8}Th$_2$Tp^8**, from the oxidative homo-coupling of **M1–M5**, respectively. Additionally, 11 other symmetrical π-bridged dimers were synthesized by the Suzuki–Miyaura coupling using monomers **M0–1**, **M0–2**, **M0–3** and **M0–4** and appropriate diboronic acid derivatives, including **Tp^{6,8}PhTp^{6,8}**, **Tp^{6,8,12}Ph$_2$Tp^{6,8,12}**, **Tp^{6,8}TtTp^{6,8}**, **Tp^{6,8}BtTp^{6,8}**, **Tp^{12}Th$_2$Tp^{12}**, and **Tp^{6}Tp^6**, with no bridge between the triphenylenes, and two compounds with unsymmetrical chain substitution patterns, **Tp^{6}Ph$_2$Tp^{12}** and **Tp^{6}Th$_2$Tp^{12}**. The thermal behavior of the monomers will be briefly discussed first, followed by the mesomorphous properties of the unsymmetrical σ-bridged dimers **Tp^{6}T^6** and **Tp^{6}Dt^6**, and finally, the mesomorphism of the complete set of π-bridged dimers, **Tp^i-π-Tp^j**.

Mesomorphism of monomers M0–M5. The removal of one alkyl chain of the hexa(alkylated) TP mesogen and its replacement by a fluorinated nonaflate segment do not suppress its self-assembling ability. Both compounds, **M0–1** and **M0–2**, display a near-ambient Col$_{hex}$ mesophase, recognized *a priori* by their optical textures that exhibit growing monodomains and large homeotropic zones (Fig. S61, ESI†), as well as a substantial improvement in mesophase stability of about 80 °C over their fully alkylated homologues, with clearing temperatures up to *ca.* 175 °C (Fig. S64 and Table S8, ESI†). Similar behaviors were previously reported for a triflate penta(hexyloxy)TP homologue (Col$_{hex}$ 173 °C Iso)[75] and other TP-nonaflate derivatives.[76] The subsequent substitution of the nonaflate group with small heterocyclic aromatic moieties yielding the monofunctionalized discogens **M1** to **M5** is not detrimental either to mesomorphism despite the loss of one lateral chain and the insertion of a bulky component. This substitution did not *a priori* change the mesophase nature as suggested by POM (Fig. S61, ESI†), and further resulted in the enhancement of its stability, with wider temperature ranges and higher clearing temperatures with respect to their fully alkylated homologues but not to the same extent as that of the nonaflate-containing triphenylenes (Fig. 1 and Fig. S64, ESI†). This mesophase stability increase, already observed for related triphenylene derivatives with alkoxy-phenyl, triphenyl-amine, phenyl-carbazole, and fluorene pending groups,[75] is likely due to the stronger and favorable intermolecular interactions induced by the enlargement of the aromatic core π-conjugation and higher orbital overlaps. The pending thiophene and furan groups were found to have similar effects on the melting and clearing temperatures of **M1–M3**, whereas for M4 with the pending thienothiophene unit, the mesophase stability was substantially enhanced (Fig. 1). Increasing the length of the lateral chains reduces slightly the transition temperatures (**M1** *vs.* **M5**). The decomposition temperatures of these compounds determined by TGA (in dynamic mode) are invariably high, above 350 °C (for the 2% weight loss) and 370 °C (for the 5% weight loss), with a negligible effect of the nature of the substituted moiety (Fig. S62, S63 and Table S7, ESI†).

In all cases, the hexagonal symmetry of the mesophases was ultimately assigned by SWAXS measurements (Fig. S67 and Table S9, ESI†). Typical X-ray patterns display only one strong and sharp fundamental small-angle reflection assigned as (10) with, at best, an additional weak higher order, (21), along two sets of wide-angle scattering profiles, a broad scattering maximum at *ca.* 4.5–5.0 Å owing to the contribution of both the liquid-like lateral distances emerging from molten chains (h_{ch}) and nonaflate segments (h_{nf}, for **M0–1** and **M0–2**) or grafted rigid aromatic moieties (h_{ar}, for **M1–M5**), respectively, and the wide-angle semi-diffuse peak at *ca.* 3.5 Å from the stacking of the triphenylene discs into columns (h_{TP}). Therefore, these triphenylene molecules stack face-to-face into columns with the pending nonaflate segments or aromatic substituents randomly distributed in the aliphatic periphery thus without contributing to nano-segregation boundaries, but producing an irregular interface with the aliphatic periphery, in agreement with the quasi absence of high-order reflections in the SWAXS patterns. The average thicknesses of the molecules, h_{mol}, deduced from the ratio between the molecular volumes and columnar cross-section areas (Table S10, ESI†), are close to the natural stacking distances between successive triphenylene cores, h_{TP}, indicative of an almost orthogonal stacking of the TP cores into cylindrical columns, with a negligible tilt ψ of about 10–20° only with respect to the symmetry plane. This tilt likely emerges from the protruding nonaflate segment or pending aromatic moiety, respectively, that requires a larger cross-section area than an aliphatic chain (DFT, Fig. S55, ESI†). The Col$_{hex}$ mesophase therefore consists of these columns arranged at the nodes of a hexagonal lattice with a mixed and random periphery of chains and nonaflate/aromatic residues homogeneously distributed between the columns (Fig. S68, ESI†).

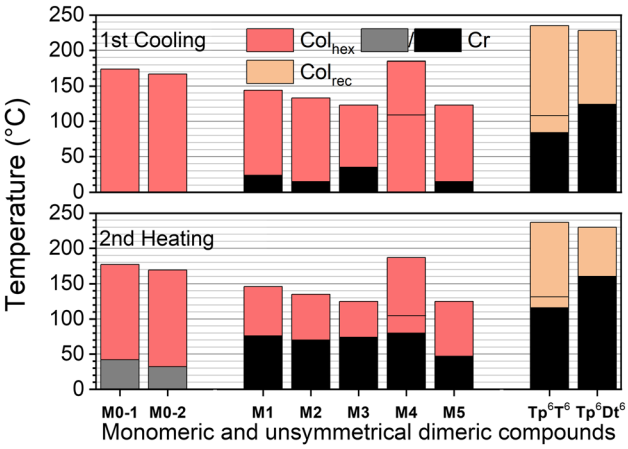

Fig. 1 Phase diagrams (top: 1st cooling; bottom: 2nd heating) of the precursors, monomeric and unsymmetrical dimeric DLCs. For **M4**, a transition between two Col$_{hex}$ mesophases was detected by DSC and POM; For **Tp^{6}T^6**, a transition between two rectangular phases was detected by DSC and SWAXS.

Mesomorphism of the unsymmetrical σ-bonded dimers, Tp^{6}T^6 and Tp^{6}Dt^6. POM texture images of the unsymmetrical dimers, **Tp^{6}T^6** and **Tp^{6}Dt^6**, differ largely from those of their parents, **M1** and **M4**, by the presence of large birefringent domains with straight edges and angular corners, suggesting a different mesophase with a reduced symmetry (Fig. S61, ESI†).

The transition temperatures were also substantially enhanced with respect to **M1** and **M4**, and the mesophases existed over broader temperature ranges from 116 to 237 °C for **Tp^{6}T^6** and 160 to 230 °C for **Tp^{6}Dt^6** (Fig. 1 and Fig. S65, ESI†). Since the melting point of **Tp^{6}Dt^6** is high, its mesophase occurs over a narrower range than that of **Tp^{6}T^6**. The onsets of decomposition were also found at higher temperatures than those of the precursory TP monomers, above 360 °C for **Tp^{6}T^6** and in the 400 °C range for **Tp^{6}Dt^6** (Fig. S62 and S63, ESI†). Between the melting and the clearing temperatures, DSC of **Tp^{6}T^6** further revealed another transition, of weaker intensity, between two mesophases, which was not detected by POM. This significant increase of both transition and decomposition temperatures obviously results from stronger intermolecular interactions induced by the extension of the π-conjugation and increased rigidity of the core after annulation, particularly true for the larger **Tp^{6}Dt^6**; the higher clearing temperatures are attributed to the enhanced segregation due to the larger number of aliphatic chains able to embed the rigid part.

As expected, from the molecular shape change, the nature of the mesophase was modified accordingly. SWAXS patterns recorded at different temperatures confirmed the change of the mesophase nature, and the formation of columnar rectangular mesophases for both compounds (Fig. S69, ESI†). Although not so well resolved, X-ray patterns reveal nevertheless two very intense small-angle peaks, assigned to (11)/(20) of a rectangular lattice, plus, for the low-temperature phase of **Tp^{6}T^6** (see below), a few other peaks of weaker intensity (Table S11, ESI†); the large-angle part reveals a broad band with two maxima (h_{ch} and h_π, from the chain and extended aromatic part, respectively). Furthermore, SWAXS confirmed the phase transition between two rectangular mesophases for **Tp^{6}T^6** and the detailed peak analysis indicated the possibility of a symmetry change, *i.e.*, *c2mm* and *p2gg*, between two Col_{rec} mesophases; the high temperature mesophase was indexed, by convention, according to the highest centered symmetry (*c2mm*), whereas the low-temperature phase was logically indexed according to the herringbone-like symmetry (*p2gg*). Recall that these two planar symmetries correspond, respectively, to the specific orientations of the elliptical columnar cross-sections within the rectangular lattices, the long elliptical axis lying along the *a*-axis for the centro-symmetric *c2mm* lattice, or alternating its orientation with respect to the same *a*-axis (Fig. 2) to form a herringbone-like arrangement for the *p2gg* one. For **Tp^{6}Dt^6**, the rectangular phase was also confirmed by the presence in the SWAXS pattern of the two fundamental reflections (11) and (20) and the two broad wide-angle signals. Since no other reflections were present, the two reflections could not be differentiated, and the symmetry of the phase could not be solved either, as above the highest symmetry has been considered (Table S11, ESI†).

The average molecular thickness, h_{mol}, in the mesophases diverges from the stacking distances between successive π-extended aromatic cores, h_π, regardless of the symmetry considered for **Tp^{6}T^6**, and indicative of tilted stacking of the rigid molecular cores, with respect to the symmetry plane (Table S12, ESI†). As confirmed by DFT simulations (Fig. S58, ESI†), these two molecules are not completely planar, with the triphenylene parts slightly tilted out of plane with respect to the thiophene-containing units, likely induced by the proximity of the aliphatic chain in the 3-position and the thiophene parts, thus affecting the stacking. Both the dimers have an average oval shape with 9 lateral chains, and their stacking somehow still preserves this shape and confers the elliptical cross-section to the columns, in agreement with the rectangular symmetry of the mesophases. This piling of the cores thus implies the periodic repartition of the central chain around the molecular cores that can be obtained by the alternated stacking of the molecules with respect to the columnar axis (*i.e.*, point symmetry inversion, Fig. 2).

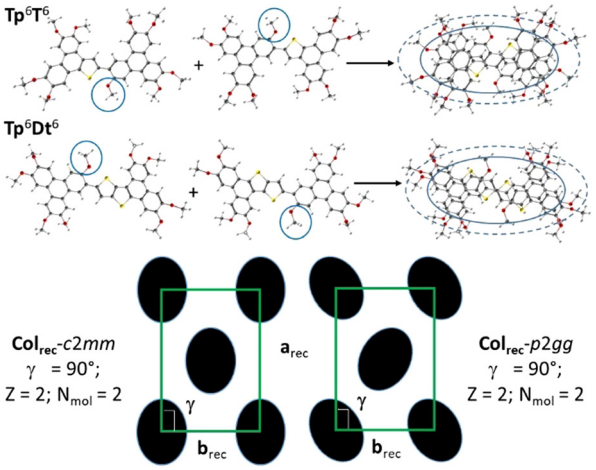

Fig. 2 Schematic representations of molecular self-assemblies and supramolecular organizations in the various mesophases of the unsymmetrical σ-dimers, **Tp^{6}T^6** (*c2mm* and *p2gg*) and **Tp^{6}Dt^6** (*c2mm*); a_{rec}, b_{rec}, γ: lattice parameters and angle, *Z*: number of columns per lattice and N_{mol}: number of mesogens per lattice; the central chain is circled in blue (the chains are not represented for clarity).

Mesomorphism of the π-bridged dimers, Tp^{i,j}-π-Tp^{i,j}. All π-bridged dimeric triphenylene compounds have high thermal stability, with decomposition temperatures above 350 °C (1% weight loss), similar to their aryl-triphenylene counterparts, with negligible effects of the chain-lengths and of the nature of the central rigid bridge, apart from **Tp^{6,8}BtTp^{6,8}**. Indeed, both terms having the two chains radiating from the central bridge stand out from this series as they decompose at a slightly lower temperature, around 325 °C (Fig. S62 and S63, ESI†). They display a clear two-stage decomposition process, with a first step (at *ca.* 300 °C) likely corresponding to the dealkylation of the central core as previously observed,[35] before following the same regime of decomposition of the other dimers. In the following, the mesomorphism behaviour will be discussed as a function of the triphenylene chain-length and bridge, **Tp^i-π-Tp^i** (i,j = 6, 8, 12), and substitution pattern, **Tp^i-π-Tp^j** (i = 6, j = 12), respectively.

All of the linear dimers **Tp^6-π-Tp^6**, thus excluding the kinked dimer **Tp^{6}β-Th$_2$Tp^6** for now (see below), exhibit liquid crystalline properties over very broad temperature ranges (Fig. 3 and Fig. S66, ESI†). They all clear reversibly into the isotropic liquid

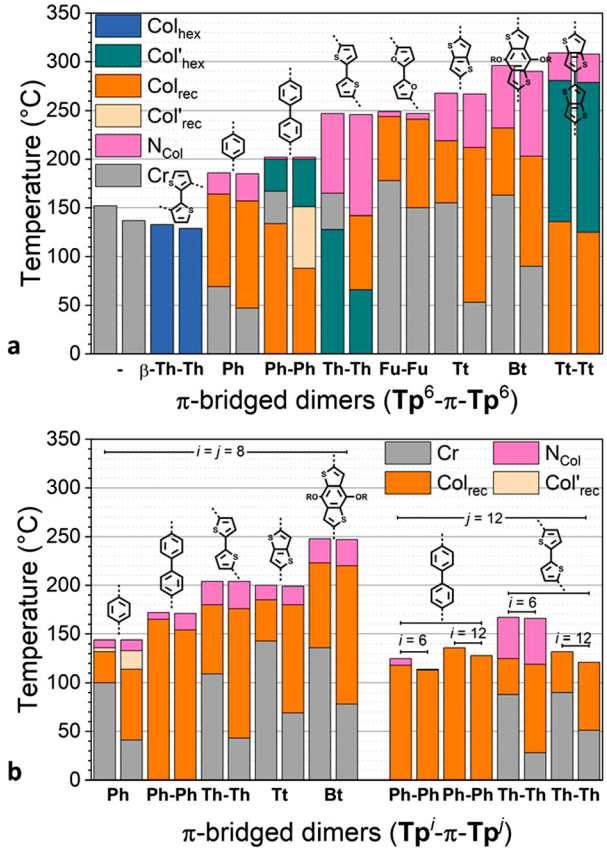

Fig. 3 Phase diagram of π-bridged discotic dimers (both 2nd heating and 1st cooling are displayed in bar diagram for each compound): (a) **Tp^6-π-Tp^6** and (b) **Tp^i-π-Tp^j** (i,j = 6, 8, 12).

at remarkably high temperatures from *ca.* 180 °C (**Tp^{6}PhTp^6**) and up to 310 °C (**Tp^{6}Tt$_2$Tp^6**), that is at much higher temperatures than their monofunctionalized triphenylene precursors (Fig. 1). This trend more or less follows the length of the bridge binding the two triphenylene moieties, *i.e.*, the longer the bridge, the higher the clearing. In contrast, the melting point does not follow this trend: some of the dimers are mesomorphous at room temperature (**Tp^{6}Ph$_2$Tp^6**, **Tp^{6}Th$_2$Tp^6** and **Tp^{6}Tt$_2$Tp^6**), **Tp^{6}PhTp^6** melts at around 70 °C, whereas **Tp^{6}Fu$_2$Tp^6**, **Tp^{6}TtTp^6** and **Tp^{6}BtTp^6** melt into liquid crystalline phases above 150 °C. Of interest, the simple ditriphenylene derivative, **Tp^{6}Tp^6**, in which both triphenylenes are directly linked, is not mesomorphous, and melts in the isotropic liquid at *ca.* 150 °C. As for the kinked dimer **Tp^{6}β-Th$_2$Tp^6**, its clearing point is similar to that of its monomeric counterpart **M2**, and is also mesomorphous at room temperature. The effect of the chain-length ($i = j$ = 6, 8, 12) and chain-repartition ($i \neq j$) is also very effective over the control of the mesophases' properties. Although the variation in the clearing temperatures mirrors the trend observed for the hexyloxy derivatives, these temperatures are significantly reduced with increasing chain-length for the octyloxy (clearing temperatures between *ca.* 145 and 250 °C) and for the dodecyloxy (132–136 °C) derivatives (Fig. 3). Similarly, compounds with non-symmetrical chain substitution patterns behave almost as their longer-chain (dodecyloxy) symmetrical homologs (125 °C for biphenylene and 167 °C for bithiophene). Thus, in these molecular systems, not only the bridge is essential in promoting mesomorphism, its chemical structure also strongly affects the transition temperatures of the dimers.

Furthermore, these dimers display a very rich and varied mesomorphism including nematic, rectangular and hexagonal columnar mesophases. On cooling from the isotropic liquid, a nematic phase is systematically induced for all the compounds, except for the kinked dimer (**Tp^{6}β-Th$_2$Tp^6**) and for the two dodecyloxy derivatives (**Tp^{12}-π-Tp^{12}**). The nematic phase was recognized by the formation of Schlieren and/or thread-like textures, and in some case by the presence of large homeotropic areas (Fig. 4 and Fig. S61, ESI†). The domain of existence of the nematic phase is intimately entailed by the nature of the chemical bridge and the chain-length but no clear trend between the type of bridge and the extension of the nematic phase could be easily established. That said, this phase occurs only over a few degrees for the biphenylene and bifuran dimers, whereas is broad for all the thiophene-containing dimers. Of interest, the two central chains in the bridge of **Tp^{6}BtTp^6** strongly promote this phase. Its occurrence was somehow not surprising as such a nematic phase has already been observed in other structurally related twin-like discotic systems.[73] Increasing the chain-length reduces the range of existence of this mesophase, except for the octyloxy biphenylene term (**Tp^{8}Ph$_2$Tp^8**). This phase is also observed for the two unsymmetrically substituted dimers, although for **Tp^{6}Ph$_2$Tp^{12}**, the domain is larger on heating than on cooling, and this is probably as a consequence of the strong supercooling effect (of nearly 10 °C) observed for this compound.

The identification of the other mesophases was ultimately achieved by SWAXS experiments carried out at different temperatures, in the range defined by DSC measurements. SWAXS patterns recorded in the nematic phase of all compounds were similar in all cases (Fig. 5 and Fig. S70, ESI†). They consisted of a strong and slightly asymmetrical small-angle diffuse signal, *D*, at about 18–25 Å depending on the bridge type and chain-length, corresponding to the mean separation between residual

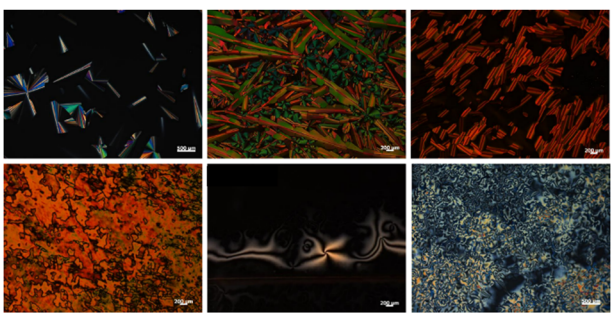

Fig. 4 Selected POM textures of some representative π-bridged dimers. Top row: **Tp^{6}β-Th$_2$Tp^6** (100 °C, Col$_{hex}$), **Tp^{6}Fu$_2$Tp^6** (228 °C, Col$_{rec}$), and **Tp^{6}Tt$_2$Tp^6** (178 °C, Col'$_{hex}$); bottom row: N$_{Col}$ of **Tp^{8}Th$_2$Tp^8** (195 °C), **Tp^{6}Ph$_2$Tp^6** (174 °C), and **Tp^{8}Ph$_2$Tp^8** (165 °C). Additional textures can be found in Fig. S57 (ESI†).

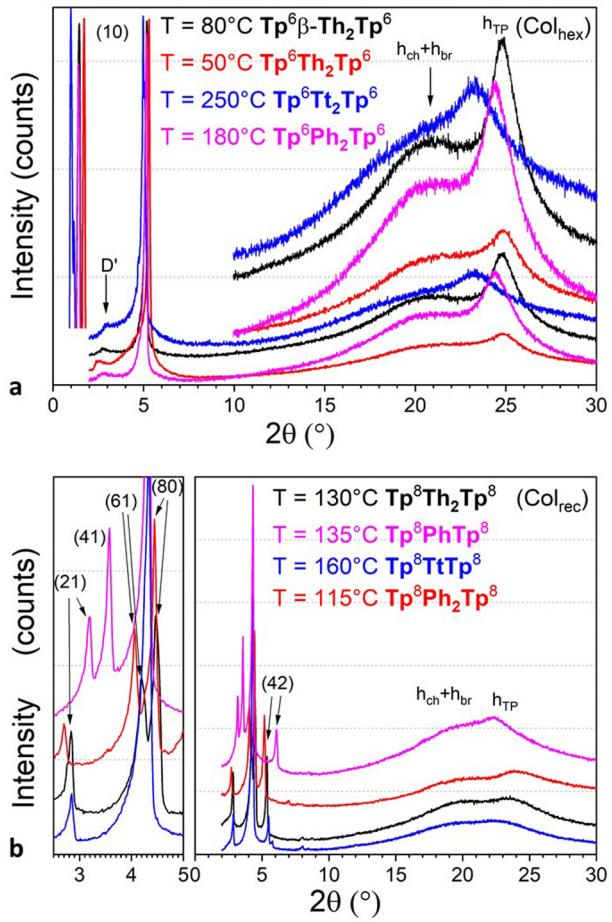

Fig. 5 Representative SWAXS patterns of some representative dimeric compounds **Tp^{i}-π-Tp^{j}** (*i,j* = 6,8) recorded at various temperatures in (a) Col$_{hex}$ (**Tp^{6}-π-Tp^{6}**, top) and (b) Col$_{rec}$ (**Tp^{8}-π-Tp^{8}**, bottom) mesophases, respectively. Only the main small-angle reflections are indexed (see Fig. S66, ESI† for all SWAXS patterns).

short-range columnar stacks, which persisted over a few molecules. In addition, one single broad and diffuse signal combining the undifferentiated contributions of the molten chains, bridges and triphenylene stackings ($h = h_{ch} + h_{br} + h_{TP}$) was observed in the wide-angle range. For some compounds, **Tp^{6}Th$_2$Tp^{6}**, **Tp^{6}PhTp^{6}**, **Tp^{6}Ph$_2$Tp^{6}**, and **Tp^{8}TtTp^{8}**, a very weak diffuse signal was also seen in the small-angle range, attributed to some reminiscent local 2D arrangement of columns in the low-orientationally ordered lattices (cybotactic groups). The maximum of the diffuse signal, observed at lower temperature, is no longer visible at the position of the h_{TP} signal. However, the asymmetrical profile of the overall low-angle region signal is consistent with the persistence of this band around 3.5–4.0 Å, indicating that the piles would still correlate but to a few molecules only. This suggests that the dimers preserve some degree of stacking, and that the columnar nematic phases, N$_{Col}$, are presumably made of short-range stacked twin-columns (Fig. 6).

On decreasing the temperature, the texture of the nematic phase gives place to different, more structured textures, as observed by POM, consisting of bâtonnet-like, fern-like or mosaic-like defects (Fig. 4 and Fig. S61, ESI†), textures which are all reminiscent of columnar phases textures, as confirmed below by SWAXS measurements (Fig. S70, ESI†). As for the nematic phase, the thermodynamic stability of the more ordered mesophases was also found to strongly depend on the bridge nature (Fig. 3). Briefly, within the hexyloxy bridged dimers set, the phenylene, bifuran, thienothiophene and benzothiophene terms all display one single columnar phase below the N$_{Col}$, over various temperature ranges, whilst the dithienothiophene shows two mesophases. The other terms behaved slightly differently. For the linear dithiophene compound, two mesophases were detected on cooling only (*i.e.* monotropic), with textures reminiscent of columnar mesophases

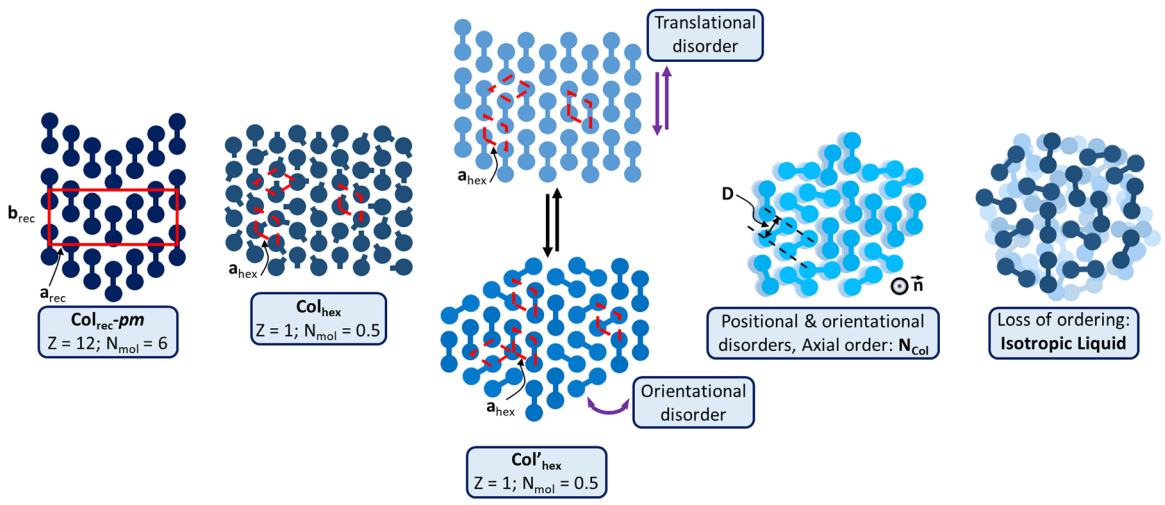

Fig. 6 Schematic representation of the various supramolecular mesomorphous arrangements induced by the π-bridged dimeric mesogens: the Col$_{rec}$-*pm* phase with chevron arrangements of the TP dimers; Col'$_{hex}$ phase, differentiated by translational or oriental order fluctuations; the Col$_{hex}$ phase of **Tp^{6}β-Th$_2$Tp^{6}** is similar to that of the monomeric precursors (Fig. S68, ESI†); the N$_{Col}$ phase characterized by loss of positional and orientational orders, but with short-range columns aligned along one main direction (axial order), the director n; isotropic liquid: no persisting molecular ordering.

(Fig. S70, ESI†), but with the low-temperature mesophase that remains stable at room temperature. On heating, crystallization occurs at ca 128°, and the nematic phase reforms at *ca.* 165 °C up to isotropisation. For the biphenylene derivative, a first mesophase is formed on cooling from the nematic phase, and on further cooling, two additional mesophases of different symmetry were also detected. As above, crystallization is induced upon re-heating the sample at *ca.* 134 °C, which melted at 165 °C in the columnar phase (Fig. 3); these two low-temperature mesophases are thus monotropic. The kinked dimer displays only one mesophase from room temperature onwards, *i.e.*, a Col_{hex} phase (Col_{hex} 133 I) as recognized by its optical texture, and later confirmed by SWAXS, and is the only dimer that does not show the nematic phase. The behavior of the longer-chain homologs is simpler and monotonous as they exhibit a single columnar mesophase below the nematic phase, the exception being the octyloxy phenylene term, which displays two mesophases.

As just mentioned, only four compounds exhibit a Col_{hex} mesophase, the kinked dimer, **Tp^{6}β-Th$_2$Tp^6**, and three linear dimers. For the kinked dimer, the mesophase is present at room temperature and up to the isotropic liquid, whereas for the other dimers, the mesophase occurs either below the nematic phase (**Tp^{6}Ph$_2$Tp^6** and **Tp^{6}Tt$_2$Tp^6**) or below the rectangular phase (**Tp^{6}Th$_2$Tp^6**). The X-ray patterns for the Col_{hex} mesophase of **Tp^{6}β-Th$_2$Tp^6** (Fig. 5) recorded on cooling from the isotropic liquid at different temperatures, display only one single but very intense small-angle reflection, indexed as the (10) reflection of a hexagonal lattice, along with the wide-angle scatterings corresponding to the mixed contribution of chains and bridges, $h_{ch} + h_{br}$, for the broad signal, and the semi-diffuse reflection characterizing the stacking of the triphenylenes, h_{TP}, respectively (Fig. 5a and Fig. S70, ESI†). The correlation length for the intense intracolumnar signal was calculated to be *ca.* 23–33 Å, decreasing with temperature, that corresponds to about 6–10 stacked TP moieties on average (for the kinked dimer). Another weak scattering, $D' \approx 30$ Å, was also seen at a lower angle, likely the sign of some evanescent superlattice (see below). The SWAXS patterns of the Col_{hex} phase for the other dimers are all very similar to that of **Tp^{6}β-Th$_2$Tp^6**, and also consist of one major intense and sharp reflection, corresponding to the fundamental reflection (10) of a hexagonal lattice, and an almost extinct, broad small-angle signal, D', as above (Fig. 5a). The wide-angle scattering was, also as for the kinked dimer, split into two distinct signals, corresponding respectively to the combined contributions of the molten chains and bridges ($h_{ch} + h_{br}$) and to the stacking of the TP cores (h_{TP}). The lattice parameter of the Col_{hex} phase of the different compounds, despite their different shapes and the nature of the bridge, is in the same range ($a_{hex} \approx 20 \pm 1$ Å, Table 1), which corresponds to one triphenylene-based column per lattice for the four dimers. This hexagonal mesophase is not induced in the compounds with small bridges, such as phenylene and thienothiophene derivatives, nor in the benzodithiophene derivatives, probably due to some steric hindrance, and is no more present in the longer-chain homologues.

All compounds, except the kinked dimer, show one or more mesophases with a rectangular symmetry. X-ray patterns recorded at various temperatures unequivocally confirmed their liquid crystalline nature (Fig. 5b and Fig. S70, ESI†), resulting from the stacking of the TP rings and the segregation between hard cores and molten chains into 1D columns. The SWAXS patterns were rather unconventional and were composed of several sharp reflections in the small-angle range with a particularly intense one, confirming the formation of long-range ordered mesophases with large superlattices of reduced symmetry (Fig. 5b). The presence of a strong and extended wide-angle signal completed the patterns. This scattering was clearly split into the distinct molecular segments' contributions; the broader scattering corresponding to the combined and undifferentiated contributions of the molten chains and bridges ($h_{ch} + h_{br}$), and the more-or-less semi-diffuse signal associated with the stacking of the TP cores (h_{TP}), respectively. Only the dimers with central chains (**Tp^{6,8}BtTp^{6,8}**) showed one single diffuse signal, corresponding to the overlap of the various molecular contributions ($h = h_{ch} + h_{br} + h_{TP}$), somehow expected since all the segments have almost identical cross-sections.

The sharp, low-angle reflections observed for most compounds were indexed within a planar rectangular symmetry (Table S13, ESI†). The overwhelming, mid-angle, single reflection, systematically present for all compounds, was ultimately assigned to the (80), whereas the other reflections were indexed as (21), (61) and (42), respectively, thus corresponding to strongly anisotropic, large two-dimensional rectangular superlattices ($a_{rec} \gg b_{rec}$, Table 1). Such an indexation of the patterns for all the dimers is entirely satisfying, particularly for the high-order reflections and for the non-symmetrically substituted compounds (see Δ in Table S13, ESI,† and below). This indexation solution gives very large and anisotropic rectangular lattices with the *a*-parameter varying between 132 and 146 Å and the *b*-parameter between 30.5 and 38.2 Å for the **Tp^6-π-Tp^6** compounds (Table 1). The *a*-parameters increase obviously with chain-lengths whereas the *b*-parameters remain quite constant throughout ($a_{rec} \approx$ 156–170 Å and $b_{rec} \approx$ 31–38 Å for the **Tp^8-π-Tp^8**, and $a_{rec} \approx$ 187–194 Å and $b_{rec} \approx$ 34–37 Å for the **Tp^{12}-π-Tp^{12}**). These large parameters imply several columns per lattice. The uneven distribution of the intensity of the reflections in this angular range and the partial or total extinction of the fundamental reflections (in this case, complete extinction of the fundamental reflections (11) and (20)), are the signature of important electronic density modulation emerging from periodic alternations between electron-rich zones (triphenylenes and bridges) and electron-poor areas (aliphatic continuum) within these large superlattices. The formation of such large superlattices of low symmetry strongly supports the formation of multicolumnar mesophases, somehow expected due to the intrinsic "dumbbell-like" shape of the mesogens. The absence of conditions on the reflections (*hk*) in most cases indicated also the formation of non-centered rectangular lattices.

The overall average intensity of the signal (h_{TP}) indicates that the overlap between successive TP rings of the same dimer is

Table 1 Structural and geometrical parameters of the columnar mesophases of the bridged dimer mesophases at various temperatures

$Tp^{i,j}$-π-$Tp^{i,j}$	T^a	Phase^b	$V_{mol}{}^c$	ρ^c	a^d	b^d	a/b^d	γ^d	A^d	$N_{mol}{}^e$	$h_{mol}{}^e$	$Z_{col}{}^e$	h_{TP} (ξ)^f/[h]	$\langle\psi\rangle^g$	$\chi_{TP}{}^h$	$\langle D_{TP}\rangle^i$	$\langle s_{ch}\rangle^j$	$\langle q\rangle^k$
$Tp^6Th_2Tp^6$	120	[Col_{rec}]	2889	0.931	134.0	35.0	3.83	90	4691.3	6	3.69	12	3.72 (9)	~0	0.274	11.68	22.60	0.99
	50	[Col'$_{hex}$]	2720	0.989	19.3	19.3	1	120	334.0	0.5	4.07	1	3.58 (15)	28	0.283	10.98	23.40	1.08
Tp^6β-Th_2Tp^6	120	Col_{hex}	2889	0.931	19.9	19.9	1	120	341.9	0.5	4.22	1	3.63 (23)	26	0.274	10.92	24.14	1.06
	80	Col_{hex}	2788	0.965	19.8	19.8	1	120	339.9	0.5	4.10	1	3.58 (31)	24	0.280	11.00	23.62	1.06
	40	Col_{hex}	2561	1.051	19.7	19.7	1	120	337.1	0.5	3.80	1	3.54 (33)	21	0.305	11.43	22.75	1.05
$Tp^6Fu_2Tp^6$	200	Col_{rec}	3111	0.848	139.1	32.1	4.34	90	4463.0	6	4.18	12	3.91 (−)	21	0.262	11.14	24.39	1.01
$Tp^6Tt_2Tp^6$	250	Col'$_{hex}$	3358	0.857	20.9	20.9	1	120	380.1	0.5	4.42	1	3.85 (13)	29	0.247	10.94	25.32	1.02
	100	Col_{rec}	2923	1.036	141.3	34.0	4.16	90	4800.7	6	3.65	12	3.55 (35)	14	0.269	11.70	22.37	0.99
Tp^6PhTp^6	120	Col_{rec}	2273	0.917	144.6	30.5	4.74	90	4404.8	6	3.78	12	3.94	—	0.286	11.55	22.86	1.00
$Tp^6Ph_2Tp^6$	180	Col'$_{hex}$	3098	0.862	19.9	19.9	1	120	343.6	0.5	4.51	1	3.66 (21)	36	0.261	10.69	25.25	1.06
	120	[Col'$_{rec}$]	2923	0.914	137.7	37.5	3.67	90	5164.4	6	3.40	12	3.59 (42)	—	0.271	12.18	21.69	0.95
	50	[Col_{rec}]	2754	0.967	132.3	38.2	3.47	90	5053.3	6	3.27	12	3.57 (32)	—	0.280	12.25	20.98	0.97
Tp^6TtTp^6	190	Col_{rec}	3006	0.881	145.9	33.8	4.31	90	4939.4	6	3.65	12	3.92 (8)	—	0.270	11.90	22.75	0.95
	80	Col_{rec}	2698	0.981	143.0	32.7	4.38	90	4673.1	6	3.46	12	3.81	—	0.289	11.97	21.69	0.98
Tp^6BtTp^6	190	Col_{rec}	3475	0.868	143.0	34.4	4.16	90	4920.6	6	4.24	12	[4.21]	—	0.234	11.05	24.53	1.02
$Tp^8Th_2Tp^8$	130	Col_{rec}	3598	0.877	157.7	36.1	4.36	90	5700.1	6	3.79	12	3.79 (−)	—	0.221	11.56	22.94	1.00
	50	Col_{rec}	3271	0.965	155.6	35.9	4.33	90	5590.7	6	3.51	12	3.67 (67)	—	0.236	11.82	21.73	1.00
Tp^8PhTp^8	135	Col'$_{rec}$	3400	0.885	163.4	32.1	5.08	90	5254.6	6	3.88	12	3.99	—	0.234	11.43	23.22	1.00
	100	Col_{rec}	3302	0.912	164.2	31.6	5.20	90	5185.8	6	3.82	12	3.95	—	0.238	11.44	22.89	1.02
	50	Col_{rec}	3155	0.954	163.9	31.0	5.29	90	5076.6	6	3.73	12	3.88	—	0.244	11.47	22.41	1.03
$Tp^8Ph_2Tp^8$	115	Col_{rec}	3488	0.899	159.0	38.0	4.18	90	6046.7	6	3.46	12	3.70 (13)	—	0.227	12.06	21.85	0.96
	50	Col_{rec}	3305	0.949	156.2	37.6	4.16	90	5869.9	6	3.38	12	3.62 (6)	—	0.233	12.05	21.33	0.98
Tp^8TtTp^8	160	Col_{rec}	3509	0.887	170.5	34.8	4.90	90	5932.7	6	3.55	12	3.83	—	0.229	12.00	22.32	0.95
Tp^8BtTp^8	200	Col_{rec}	4048	0.860	163.8	34.8	4.71	90	5698.3	6	4.26	12	[4.30]	—	0.201	11.04	24.62	1.02
	100	Col_{rec}	3684	0.945	162.9	34.8	4.68	90	5669.8	6	3.90	12	[4.28]	—	0.13	11.33	23.13	1.03
$Tp^6Th_2Tp^{12}$	105	Col_{rec}	4099	0.827	182.8	34.2	5.34	90	6260.9	6	3.93	12	3.68	20	0.192	11.30	23.24	1.03
	50	Col_{rec}	3664	0.925	177.6	34.4	5.16	90	6107.7	6	3.60	12	3.62	—	0.210	11.68	22.01	1.01
$Tp^{12}Th_2Tp^{12}$	110	Col_{rec}	4590	0.891	187.3	34.4	5.44	90	6446.2	6	4.27	12	3.71	29	0.172	10.84	24.24	1.07
$Tp^6Ph_2Tp^{12}$	100	Col_{rec}	4084	0.825	173.3	36.0	4.82	90	6231.1	6	3.93	12	3.72	19	0.192	11.21	23.06	1.02
	50	Col_{rec}	3698	0.911	173.1	35.1	4.93	90	6078.2	6	3.65	12	3.62	7	0.208	11.59	22.16	1.02
$Tp^{12}Ph_2Tp^{12}$	110	Col_{rec}	4624	0.880	194.4	37.3	5.21	90	7256.9	6	3.82	12	3.76	10	0.171	11.47	22.95	1.01
	50	Col_{rec}	4408	0.923	193.6	37.3	5.20	90	7213.5	6	3.67	12	3.66	0	0.175	11.57	22.23	1.02

^{a} Temperature of the experiment (°C). ^{b} Mesophase type, square brackets refer to the monotropic phase. ^{c} Molecular volume (Å^3) and density (g cm^{-3}) calculated by additivity of partial elementary volumes: $V_{mol} = V_{TP} + V_{br} + V_{ch}$, the sum of the volume of the TP and bridge parts (from reference compounds) and volume of the chains, V_{ch}, see ref. 82; $\rho = M_W/(N_A V_{mol})$. ^{d} Lattice parameters a, b and γ (Å, °) and cross-section areas A (Å^2): Col_{hex}, $a = b = a_{hex}$, $A = a^2 \sin\gamma$; for Col_{rec}: $a = a_{rec}$, $b = b_{rec}$, $A = a \times b$; a/b: anisotropic ratio. ^{e} Number of molecules per lattice, N_{mol}, columnar slice thickness, $h_{mol} = V_{mol} \times N_{mol}/A$ (Å), and number of columns per lattice, $Z_{col} = N_{mol} \times n_{TP}$, where n_{TP} is the number of TP per molecules (*i.e.* $n_{TP} = 2$). ^{f} Face-to-face π–π stacking distance, h_{TP}, (Å) from scattering maximum from the SWAXS pattern, and ζ, correlation length (Å) determined using the Debye–Scherrer formula; h: undifferentiated liquid-like contributions of the chains, bridges and triphenylene moieties. ^{g} Out-of-plane tilt angle ψ(°) of TP mesogen cores inside columns: $\psi = \arccos(h_{TP}/h_{mol})$. ^{h} Triphenylene volume fraction ($\chi_{TP} = V_{TP}/V_{mol}$). ^{i} Average TP diameter of equivalent circular columnar core cross-sectional area: $\langle D_{TP}\rangle = [(4 \times A \times \chi_{TP})/(Z_{col} \times \pi)]^{1/2}$. ^{j} Average cross-section area per chain per TP unit: $\langle s_{ch}\rangle = \pi\langle D_{TP}\rangle \times h_{mol}/6$ (5 chains + 1 bridge). ^{k} Chain packing ratio: $\langle q\rangle = \langle s_{ch}\rangle/\sigma_{ch}$, σ_{ch} being the available cross-sectional area for a molten chain ($\sigma_{CH_2} = V_{CH_2}/1.27$), ref. 82.

not infinite but still predominates and extends to several stacks; this limitation is likely due to some distortion imposed by a slight twist of the bridges and/or their bulkiness with respect to the two adjacent triphenylene moieties (see DFT calculations, Fig. S58, ESI†). Although the stacking between the triphenylenes appears perturbed, as evidenced by the enlargement of the h_{TP} stacking signal, the correlation length for the intracolumnar stacking could nevertheless be calculated for some compounds from the peak thickness at mid height using the Debye–Scherrer formula, providing that the reflection was sufficiently sharp. These calculations show that the correlation length was *ca.* 35 ($Tp^6Tt_2Tp^6$), 42 ($Tp^6Ph_2Tp^6$) and 67 Å ($Tp^8Th_2Tp^8$), which correspond to about 10–20 stacked TP moieties for these most ordered systems. The persistence of this signal (h_{TP}) for most compounds in the mesophase is also a further indication that this stacking is preferentially intracolumnar (the dimers would stack into discrete double cable columns in this case) rather than intercolumnar (undifferentiated stacking of TPs with connections between neighboring dimers), which would lead to unfavorable mixing between aromatic cores and lateral chains.

The two enantiotropic phases of Tp^8PhTp^8, detected below the nematic phase (Fig. 3), showed similar patterns to the rectangular phases described above, with an intense mid-angle reflection that could be indexed also as the (80), plus additional weaker reflections, and split wide-angle scattering. The only difference between these two mesophases was the emergence in the high-temperature phase of another reflection indexed as (81), likely corresponding to slight orientational changes of the dimers with respect to the lattice axes. As for the two monotropic phases of $Tp^6Ph_2Tp^6$, detected below the high-temperature Col_{hex} phase, slightly different X-ray patterns were obtained, but still preserving some of the common features already described above; differences mainly occur in the mid-angle range (Fig. S70 and Table S13, ESI† for details of the indexation).

Therefore, and not so surprisingly, all these dimeric compounds exhibit a rich mesomorphism, whose induction is strongly driven by the tendency of the triphenylene units to stack into one-dimensional twin-columns and, for the 2D phase, to further nanosegregate in space due to the peripheral alkyl chains. The relative arrangement of the twin-columns into rectangular (and single column for the hexagonal) lattices however is not straightforward, and is somehow controlled by the geometrical constraints imposed by the bridge. As previously developed,[11,34,35] more intimate details about the respective organization of the columns within the superlattices can be revealed in part. The ratio between the molecular volume (V_{mol}) and the lattice area (A), scaled by the total number of dimers per lattice, N_{mol}, according to the formula, $h_{mol} = [V_{mol} \times N_{mol}]/[A]$ (Table 1), simultaneously provides N_{mol} and a value for h_{mol}, the molecular slice thickness, after successive trial and error loops, and keeping the most viable solution in agreement with the symmetry elements of the planar group and the various geometrical constraints (Table 1). Here, for the rectangular phases, N_{mol} was found to converge to 6 dimers, which correspond to columnar rectangular superlattices containing 12 TP-based single columns ($Z_{col} = 2 \times N_{mol}$, for a molecular slice thickness value h_{mol} that lies in the vicinity of the stacking periodicity along the TP-based columns, h_{TP}). For the Col_{hex} phases, these calculations give half a dimer that corresponds to the self-assembly of 1 TP-based columns (Table 1). As discussed above for the monomeric precursors, the average thickness of the molecules, h_{mol}, is also close to the stacking distance between successive triphenylene cores, h_{TP}, indicative of an almost orthogonal piling of the TP cores into cylindrical columns.

The striking feature commonly observed in all the SWAXS patterns of the Col_{rec} mesophase is the systematic presence of the very intense, mid-angle reflection, (80), which is located at the same angle to that of the intense fundamental reflection (10) of the Col_{hex} phase (of the triphenylene precursors and some dimers). As recalled from above, the natural tendency of TP mesogens is to stack into perfectly cylindrical columns that sit at the nodes of a hexagonal lattice, in order for the chains to homogeneously fill the available space. This suggests that an underlying similar local hexagonal arrangement of the almost cylindrical individual columns of each dimeric system is likely preserved in the rectangular phases, although at the local range, and that the reduction of the symmetry of the mesophases is imposed by the respective positional, translational and orientational orderings of the bridges connecting both TP units with respect to each other. Here, in a first simple approximation, it is assumed that the discs are located at the nodes of a pseudo hexagonal net, with the spacing being determined by the bridge and chains lengths, in order for the chains to fully fill the available space. This would then lead to a kind of staircase-like arrangement of the dimers, with one of the triphenylene part facing the bridge of its neighbor, arrangement that would be further facilitated by the absence of chains around the bridge. The self-assembling of the 6 dimers (*i.e.* 12 columns) according to a seamless zigzag chevron pattern is proposed that satisfies both lattice parameters and molecular dimensions. It is therefore possible to arrange the 6 dimers side-by-side in each chevron, with one TP unit interlocking into the free space left by the bare bridge of its close neighbors, and with all the TP units being equally spaced (*i.e.*, as in a pseudo hexagonal net), and obviously depending on the bridge type. In other words, the molecules fit together like the pieces of a puzzle to maximize the density of the packing. The rectangular symmetry implies first the periodic change of the staircase direction at mid-lattice length (Fig. 6 and Fig. S72, ESI†), and second, that each chevron has to be separated from one another by a distance which is different from the TP–TP distance within the chevron. Under these conditions, this arrangement satisfies the symmetry and geometrical criteria outlined above, and gives a 2D tiling with the *pm* rectangular symmetry (no conditions on the *hk* reflections). This model is further supported by the packing chain ratio which is close to unity (Table 1). The other rectangular mesophases present in this system may involve tiny modifications, such as a slight tilt of the triphenylene discs with respect to the *b*-axis. Obviously, a deeper study, *e.g.* molecular modelling, correlating the separations between each chevron and between each neighboring dimer in the chevrons as a function of the length of the alkoxy chains irradiating from the TP cores and the length of the bridges, respectively, with the mesophase formed (Fig. 6 and Fig. S72–S74, ESI†), would support this model proposal and give other valuable information, but such investigations have not yet been realized.

DFT calculations (Fig. S58, ESI†) reveal that in the case of the kinked dimer, the bithiophene bridge favors the segregation between the aromatic core and chains by forcing the two TP units to almost lie on top of each other to form a pseudo cylindrical subunit likely at the origin of the induction of the Col_{hex} mesophase. Structural and geometrical parameters agree with the formation of such types of single triphenylene-based columns (Table 1) and that half-twin **Tp^6β-Th_2Tp^6**, *i.e.*, one triphenylene core fits within the hexagonal lattice. The folded bridge however obviously protrudes out of the cylindrical core, thus reducing the free rotation of the overall dimer around the columnar axis and responsible for the irregular chain–core interface, explaining partly the absence of higher reflection orders. **Tp^6β-Th_2Tp^6** thus self-assembles in the same kind of Col_{hex} mesophase as its monomeric precursors (Fig. S64, ESI†). The evanescent superlattice of reduced symmetry would then arise from the random orientation of the folded bridge (Fig. 6).

For linear dimers showing the hexagonal phase, the rigid bridges connecting the two triphenylenes do not bend and thus, the supramolecular organization in the Col_{hex} phase is expected to be different from that of the kinked dimer. However, the hexagonal lattice parameters also agree with the formation of one triphenylene-based column as for the kinked dimer. The formation of the hexagonal columnar mesophases therefore necessarily results from the exact positioning of each triphenylene moiety at the nodes of a hexagonal network, with the basic unit being half of a twinned column. The formation of this mesophase stemming, on cooling, from the columnar nematic phase (for compounds **$Tp^6Tt_2Tp^6$** and **$Tp^6Ph_2Tp^6$**)

must somehow preserve some features of this phase, *i.e.*, some of the orientational disorder of the twinned columnar piles relative to the bridge axis. Then, upon continuing cooling, the molecules probably continue to rearrange so that their major axes are parallel, which is the premise for the transition to the Col_{rec} phase at lower temperatures. In this case, this intermediate phase would thus play the role of a template between these two mesophases (N_{Col} and Col_{rec}), and may be referred to as a transitory hexagonal (Col'_{hex}, Fig. 6). However, for that stemming on cooling from the rectangular phase (compound **$Tp^6Th_2Tp^6$**), the molecules likely retain some of the longitudinal ordering (see above), and would only differ by some degrees of translational disorder (along the bridge axis) to break the chevrons (Fig. 6). The formation of the low-temperature hexagonal mesophase of **$Tp^6Th_2Tp^6$** may be simply driven by the decrease in the chain fluidity. In both situations, the phase symmetry is increased and averaged to hexagonal (Fig. 6), but the core-chains interface is obviously not well defined, in agreement with the absence of high order reflections. It is also important to note that the TP stacking is preserved, suggesting persistent intercolumnar interactions. On further heating, the loss of translational order combined with the loss of orientational order of either Col_{rec} or Col_{hex} phases, respectively, actually prefigure the emergence of the nematic columnar phase which partially starts to lose the positional order of the columns upon chain dilation. The position of the broad scattering corresponding to the accumulation of the three main molecular contributions (chains, bridges and TP stacking) implies that some local intermolecular stacking is still present. The asymmetrical shape of the small-angle diffuse signal, *D*, also indicates that some local short-range ordering is persisting in the mesophase. Based on these observations, the nematic can be described as being made of twin-columns whose director is defined by the column's long axis (Fig. 6).

The chevron-like arrangement proposed above for the dimer organization within the rectangular superlattices was partially supported, at least the seeding of this arrangement, by scanning tunneling microscopy (STM), a powerful technique used to directly visualize single molecules on surfaces.[83] The variation of the tunneling current in STM allows indeed visualizing the positions and distribution of the molecules directly at the atomic level without damaging the samples.[84] The high-resolution STM images directly supply two-dimensional (2D) self-assembled patterns of molecules, and may support the self-organized patterns of the bulk, soft and disordered liquid crystalline materials in the mesophase, deduced by SWAXS. The mesomorphic character also further allows the spontaneous healing of self-organization defects and the development of long-range correlated segregated arrangements after thermal annealing and slow cooling of the samples. In addition, since most electronic devices are supported by a conductive substrate, the interfacial region between the substrate and the organic semiconductor is of significant importance, and although many favorable characteristics are reflected in the stacking direction constructed by π-conjugated systems, the behavior of these molecules on two-dimensional substrate should not be ignored.

Here, two samples, chosen as representative examples, namely **$Tp^6Tt_2Tp^6$** and **$Tp^8Th_2Tp^8$**, were dissolved in 1-phenyloctane at concentrations less than 10^{-4} mol L^{-1}. Then 2 μl of the solutions were placed on the fresh and clean highly oriented pyrolytic graphite (HOPG) surface for STM imaging. The STM tip (Pt/Ir, 80/20) was sharpened by mechanical cutting, and the detailed experiment conditions are labeled under the corresponding STM images (Fig. 7 and Fig. S71, ESI†). Detailed arrangements of the 2D self-assemblies of both π-dimers **$Tp^6Tt_2Tp^6$** and **$Tp^8Th_2Tp^8$**, at the solid/liquid interface are presented in Fig. 7 and Fig. S71, ESI.† Large scale STM images reveal that these dimers are self-assembled into monolayer nanopatterns and arranged into long-range ordering structures. The shift or tilt of the molecules is essentially due to the crowded triphenylene units that are almost facing the bare bridge parts of the neighboring molecules to maximize the packing arrangement. Due to the large π-conjugated subunits constituting the dimers, each segment interacts with the HOPG substrate *via* very strong π–π interactions, while the peripheral alkyl side chains interact with the solvent 1-phenyloctane *via* van der Waals interactions. The images show that the thermodynamic stability of the patterns depends mainly on the interactions of the functional molecules/substrate, molecule/molecule, and molecule/solvent.

Both dimeric molecules could form stable 2D nanostructures on the HOPG substrate and high-resolution STM images could then be easily obtained. These high-resolution STM images reveal that both the dimers **$Tp^6Tt_2Tp^6$** and **$Tp^8Th_2Tp^8$** are highly ordered, regularly aligned in parallel rows with well-organized 2D arrangements. In the high resolution STM image of the **$Tp^6Tt_2Tp^6$** structure (Fig. 7c), each brightened rod was assigned to one **$Tp^6Tt_2Tp^6$** molecule with the length of one molecule measured to be about 2.7 ± 0.1 nm. The oblique unit

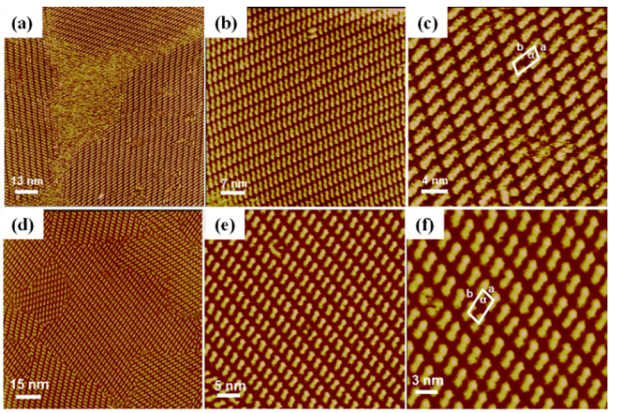

Fig. 7 Large-scale (a), medium range (b) and high-resolution (c) STM images of the self-assembly structure of **$Tp^6Tt_2Tp^6$** on the 1-phenyloctane/HOPG interface (imaging parameters: (a): I_{set} = 299.1 pA, V_{bias} = 699.8 mV; (b): I_{set} = 247.2 pA, V_{bias} = 847.2 mV; and (c): I_{set} = 299.1 pA, V_{bias} = 699.8 mV); large-scale (d), medium range (e) and high-resolution (f) STM images of the self-assembly structure of **$Tp^8Th_2Tp^8$** on the 1-phenyloctane/HOPG interface (imaging parameters: (d): I_{set} = 271.6 pA, V_{bis} = 770.0 mV; (e): I_{set} = 271.6 pA, V_{bis} = 770.0 mV; and (f): I_{set} = 271.6 pA, V_{bis} = 770.0 mV).

cell is highlighted in Fig. 7c and defined by the parameters, a = 2.3 ± 0.1 nm, b = 3.4 ± 0.1 nm, and α = 68 ± 1°. Similarly, high resolution STM images of **Tp^{8}Th$_2$Tp^8** dimers (Fig. 7f) also exhibit an oblique unit cell for the self-assembled 2D structure with similar parameters (a = 2.1 ± 0.1 nm, b = 3.6 ± 0.1 nm, α = 70 ± 1°, and with **Tp^{8}Th$_2$Tp^8** length of *ca.* 2.2 ± 0.1 nm). Thus, the above STM results agree well with the molecular lengths of both **Tp^{6}Tt$_2$Tp^6** and **Tp^{8}Th$_2$Tp^8**, which possess either longer π-bridge (**Tt$_2$** > **Th$_2$**) or shorter peripheral chains (C_6H_{13} *versus* C_8H_{17}), respectively. The molecular arrangement in the interfacial region is remarkably comparable to that of the chevron model proposed for the columnar sub-lattice of the bulk structure in the Col_{rec} mesophase for both dimers **Tp^{6}Tt$_2$Tp^6** and **Tp^{8}Th$_2$Tp^8**. In both cases, the molecules lie more or less parallel to each other, with a slight shift along their main axis in order to accommodate the hairy part (TP rings) near the naked bridges to optimize packing. The segregation pattern and the alternating row structure is thus very similar in both cases, except that both in-plane packing directions are long-range correlated in the film, whereas it is periodically alternated in the mesophase. Moreover, the lattice parameters (Table 1) are not excessively different: for **Tp^{6}Tt$_2$Tp^6**, b_{rec} = 34 Å, and $a_{rec}/6 \approx 23.5$ Å, and for **Tp^{8}Th$_2$Tp^8**, b_{rec} = 36 Å, and $a_{rec}/6 \approx 26.0$ Å; the 3D bulk organization is a fluid mesophase and involves dynamics with rotations and translations of the molecules, whereas chain-interdigitation occurs on the HOPG substrate. STM therefore kind of supports the self-organized patterns of the liquid crystalline mesophase deduced by SWAXS measurements and geometrical data analysis.

Photophysical properties and DFT results

The photophysical properties of these new compounds were studied by UV-vis absorption in solution and fluorescence emission in both solution and thin film states (Fig. 8), and the detailed parameters are provided in Table 2. The investigation of these photophysical properties of both isolated single molecules (molecular electronic structures, frontier orbitals and energy levels) and aggregated states is essential for the estimation of the potential performances and applications of organic electronic materials in OLEDs and OPVs.

In solution, the discotic monomers display absorption bands in the UV and deep-blue wavelength region (Fig. S50 and Table S1, ESI†). The absorption maxima (278–294 nm) are slightly redshifted in connection to the substituent moiety grafted onto the TP ring, increasing in the order **M0** → **M2** → **M1**(5)/**M3** → **M4**; the chain-length has no effect on these values. Their fluorescence emission maxima in solution are centered in the narrow range of 350–450nm, with redshifts of the maxima following the same order of substitution as above (and no effect of chain-length either). The solid film emission spectra of the monomers are shifted to longer wavelength than the emission in solution, up to 490 nm, due to the enhancement of the intermolecular interactions attributed to the increase of the intramolecular π-conjugation system. For instance, thin film of **M3** (containing the furan group) shows the most important red-shifted and broadest emission band, centered at nearly 500 nm, whilst **M4** (with the 2-thieno[3,2-*b*]thiophene moiety) shows a broad emission band centered at *ca.* 460 nm. Isomerism (**M1** *vs.* **M2**) and chain-length (**M1** *vs.* **M5**) also affect the maximum emission wavelength of thin films. The emissions of the thiophene-containing compounds are found below 450 nm, with the isomer **M2** even down to 400 nm. Among the functionalized discotic monomers, **M3** and **M4** also displayed the highest absolute quantum yields in solution: 25% and 30%, respectively.

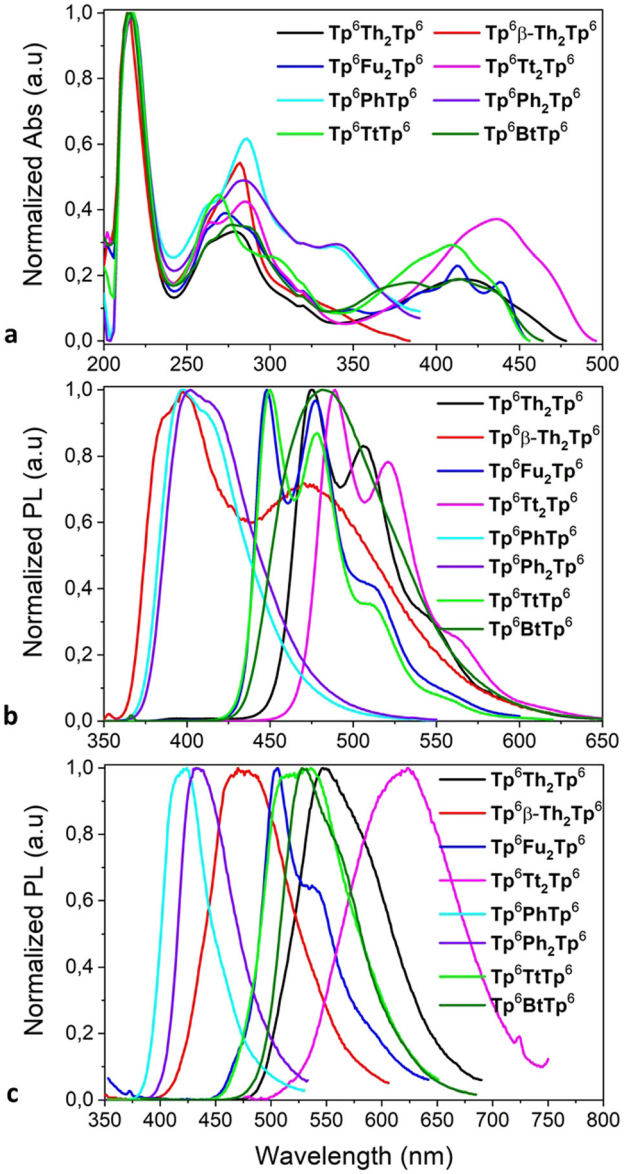

Fig. 8 (a) UV-Vis absorption spectra, (b) fluorescence emission spectra in solution, and (c) thin film fluorescence emission spectra of various π-bridged dimers.

As expected, the corresponding π-bridged dimers retain some of the absorption features of their parent compounds **M1–M4** (Fig. 8a): the first main absorption band in the range between 250 and 350 nm does not change much upon dimerization, but the bands around 350 nm are shifted to above

Table 2 Summary of the UV/vis absorption[a] and fluorescence spectroscopic properties of the dimeric compounds in solution[b] and films[c]

Compound	λ_{abs}[a]	ε[a]	λ_{em}[b]	λ_{em}[c]	Φ[d]
Tp^{6}Th$_2$Tp^6 (**Tp^{8}Th$_2$Tp^8**)	214	28.73 (28.43)	475	547 (545)	30.47 (29.82)
	264	8.67 (11.39)	506 (507)		
	278	9.59 (12.57)	545		
	320	3.12 (4.02)			
	416	5.43 (7.20)			
Tp^{6}β-Th$_2$Tp^6	214	33.57	385	470	2.28
	282	18.26	397		
	320	4.80	470		
Tp^{6}Fu$_2$Tp^6	216	25.54	448	506	66.27
	262	8.68	477	537	
	272	9.96	513		
	288	8.62			
	320	3.92			
	350	2.46			
	390	3.80			
	412	5.88			
	438	4.62			
Tp^{6}Tt$_2$Tp^6	216	27.10	489	623	36.26
	264	9.82	521		
	284	11.51	563		
	320	4.06			
	436	10.09			
Tp^{6}PhTp^6 (**Tp^{8}PhTp^8**)	216 (218)	27.38 (26.98)	398	424 (422)	44.81 (44.80)
	264	9.89 (11.24)	410		
	286	15.89 (17.99)			
	338	5.93 (6.79)			
Tp^{6}Ph$_2$Tp^6 (**Tp^{8}Ph$_2$Tp^8**)	218	26.78 (26.41)	402 (401)	434 (431)	48.41 (48.93)
	266	9.74 (10.65)	413 (412)		
	284	12.11 (13.15)			
	340	6.50 (7.13)			
Tp^{6}TtTp^6 (**Tp^{8}TtTp^8**)	218	26.28 (26.66)	450	517 (–)	53.80 (52.48)
	270	11.72 (11.69)	478	536 (569)	
	300	6.80 (6.80)	510 (509)		
	410	7.71 (7.51)			
Tp^{6}BtTp^6 (**Tp^{8}BtTp^8**)	216	29.18 (29.11)	481	532 (531)	17.30 (17.82)
	264	8.94 (9.77)		563 (562)	
	276	10.37 (11.34)			
	386	5.28 (5.75)			
	414	5.58 (6.06)			

[a] UV-vis absorption measured in the THF solution at a concentration of 1×10^{-5} mol L^{-1} (maximum absorption, λ_{abs} in nm, ε, absorption coefficient, in $\times 10^4$ L mol^{-1} cm^{-1}). [b] Emission (λ_{em} in nm) in THF solutions at a solution concentration of 1×10^{-5} mol L^{-1}. Excitation wavelength: 290 nm for **Tp^{6,8}Th$_2$Tp^{6,8}**; 320 nm for **Tp^{6}β-Th$_2$Tp^6**; 270 nm for **Tp^{6}Fu$_2$Tp^6**; 271 nm for **Tp^{6}Tt$_2$Tp^6**; 268 nm for **Tp^{6,8}PhTp^{6,8}** and **Tp^{6,8}Ph$_2$Tp^{6,8}**; 280 nm for **Tp^{6,8}TtTp^{6,8}**; and 367 nm for **Tp^{6,8}BtTp^{6,8}**. [c] Emission (λ_{em} in nm) in thin films. The thin films were obtained by drop-casting dilute THF solution and evaporation of solvent. Excitation wavelength: 350 nm for **Tp^{6,8}Th$_2$Tp^{6,8}**; 320 nm for **Tp^{6}β-Th$_2$Tp^6**; 340 nm for **Tp^{6}Fu$_2$Tp^6**; 380 nm for **Tp^{6}Tt$_2$Tp^6**; 268 nm for **Tp^{6,8}PhTp^{6,8}** and **Tp^{6,8}Ph$_2$Tp^{6,8}**; 330 nm for **Tp^{6}TtTp^6**; 340 nm for **Tp^{8}TtTp^8**; and 367 nm for **Tp^{6,8}BtTp^{6,8}**. [d] Quantum yields (Φ) in % were measured at a solution concentration of 1×10^{-5} mol L^{-1} in THF excited at different wavelengths (with the same excitation wavelengths used for[b]). Values in brackets are for the octyloxy **Tp^8-π-Tp^8** homologs, only quoted when different. Data for unsymmetrical dimers (**Tp^{6}T^6** and **Tp^{6}Dt^6**) are quoted in Table S2 (ESI).

400 nm for **Tp^{6}Th$_2$Tp^6**, **Tp^{6}Fu$_2$Tp^6**, **Tp^{6}Tt$_2$Tp^6** and **Tp^{6}TtTp^6**; the kinked dimer **Tp^{6}β-Th$_2$Tp^6** presents quasi identical features to its monomer parent **M2**. The same observations can be made for emission, for which the emission maximum is systematically redshifted in both solutions and films (Fig. 8b and c), with the larger shifts in the films (see for example **M4** *versus* **Tp^{6}Tt$_2$Tp^6**, the shift is about 200 nm).

Isomers **Tp^{6}Th$_2$Tp^6** and **Tp^{6}β-Th$_2$Tp^6** displayed different absorption and emission behavior due to their different connection patterns: in solution they show a combination of folded monomeric and extended dimeric conformation related emissions, while in the solid film only π-local monomeric emission is observed. The emission quantum yield (Φ) of **Tp^{6}Th$_2$Tp^6** is 30% with a peak at 547 nm, while for the isomer **Tp^{6}β-Th$_2$Tp^6**, the Φ value is only 2% at 470 nm. It was noted that the highest Φ value of 66% was measured for the bifuran-bridged dimer **Tp^{6}Fu$_2$Tp^6**, which showed almost identical absorption and emission spectra to that of **Tp^{6}Th$_2$Tp^6**, probing that they have similar π-electron conjugation. **Tp^{6}Tt$_2$Tp^6**, the longest π-bridged dimer, exhibits red-shifted wavelength of absorption and emission and an improved Φ value to 36%. As for **Tp^{8}Th$_2$Tp^8**, homologue of **Tp^{6}Th$_2$Tp^6**, it exhibits the same electronic spectra and Φ value, expected since the length of the peripheral alkyl chain has less or no effect on the photophysical properties. The absorption and fluorescence emission of the other dimers (Fig. 8a and b) showed a similar tendency: the thiophene-fused bridge systems **Tp^{6,8}TtTp^{6,8}** exhibit red-shifted absorption and emission compared to the phenyl-/biphenyl-bridged dimers **Tp^{6,8}PhTp^{6,8}**/**Tp^{6,8}Ph$_2$Tp^{6,8}**; their solid-state emission being further shifted to longer wavelength

than that of their solution spectra. Unsymmetrical σ-bonded discotic dimers **Tp^{6}T^6/Tp^{6}Dt^6** show red-shifted absorption and emission with Φ of 45%, due to the larger bithienothiophene-fused core (Fig. S51, ESI†).

The density functional theory (DFT, method: B3LYP, basis set: 6-31G*) method was used to calculate the frontier molecular orbital (FMO) distribution, energy levels and gaps for the methoxy homologs of these π-bridged dimers and precursors (Fig. 9 and Fig. S56, S57, S59, ESI†). Compared with the TP nonaflate **M0**, the discotic monomers **M1–M4** show narrowed HOMO–LUMO energy gaps (ΔE_{gap}) due to the obvious increase of the HOMO energy levels, caused by π-conjugation extension. The isomeric **M1** and **M2** display an obvious ΔE_{gap} difference of 0.2 eV; for **M1** with α-substitution, the thiophene moiety is better conjugated with the TP core, thus showing a narrowed energy gap than for **M2**. The furan monomer **M3** shows a similar calculated electronic structure to the thiophene monomer **M1**. Among the discotic monomers, the fused dithiophene **M4** has the most extended π-system and conjugation, showing lowered LUMO and most narrowed ΔE_{gap} (3.76 eV) compared with the TP nonaflate (4.22 eV). The DFT results (Fig. S56 and S57, ESI†) are coincident with the photophysical properties measured for the discotic monomers at the single molecular state in diluted solution.

The DFT computational results for the discotic dimers (Fig. 9 and Fig. S59, ESI†) are also consistent with the experimental measurements. For the kinked molecular structure, **Tp^{6}β-Th$_2$Tp^6** exists as a twisted conformer with reduced π-conjugation, while all the other discotic dimers possess an extended conformation with a tendency for the aromatic cores and π-bridge to lie in the same plane. **Tp^{6}β-Th$_2$Tp^6** shows theoretically the largest ΔE_{gap} (4.06 eV), just slightly narrower than that of its monomer **M2** (4.19 eV). Then, the phenyl/biphenyl bridged dimers **Tp^{6}PhTp^6** (3.99 eV) and **Tp^{6}Ph$_2$Tp^6** (3.95 eV) displayed partial π-conjugation in the single molecular state due to some degrees of rotation existing between the TP cores and the bridge. While the discotic dimer with the smallest ΔE_{gap} (2.94 eV) was **Tp^{6}Tt$_2$Tp^6**; this value is obviously smaller than that of the monomer **M4** (3.76 eV). The other thiophene/furan fused/bridged dimers also displayed narrowed ΔE_{gap} compared with that of their monomers (Fig. 9), due to the increase of the HOMO and lowering of the LUMO levels, respectively, upon the extension of π-conjugation. These DFT calculated electronic properties therefore agree fairly well with the measured photophysical behaviors of absorption and fluorescence emission.

In summary, the discotic monomers and dimers reported here show tailored π-conjugation systems and finely tuned HOMO–LUMO energy levels and gaps, color absorption and fluorescence emission; they are potential, highly valued electronic materials for further device fabrication.

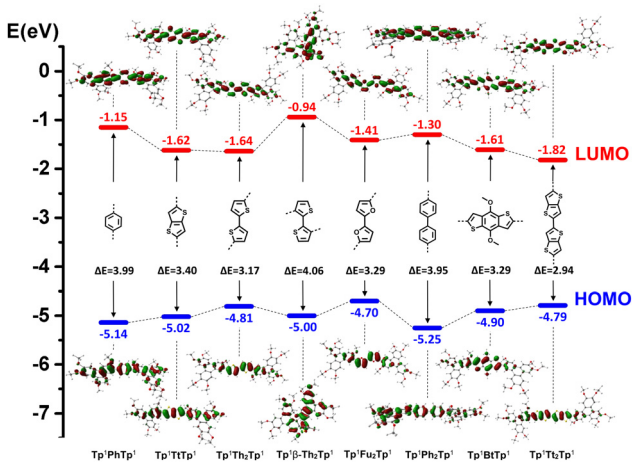

Fig. 9 HOMO–LUMO and energy gaps of the discotic dimers.

Gelling behavior of discotic dimers

Gel is an interesting type of soft matter and has tremendous industrial applications.[85] Organic π-gelators can be defined as polycyclic aromatic hydrocarbons (PAH) which dissolve first into an organic solvent when heated, then that self-assemble into one-dimensional supramolecular structures, entangle into fibers and cross-link into networks, immobilizing the solvent molecules on slow cooling. It was observed that the larger and the more planar the π-conjugated scaffold, the stronger the gelation ability. The extension of the π-conjugation and the strong intermolecular π–π interactions in these synthesized discotic dimers resulted in aggregation in solution as for other PAHs[34–36] and in the formation of gels (Fig. 10 and Fig. S53, ESI†).

The gelling properties of these π-conjugated discotic systems are determined by the nature of the bridge and the peripheral chain length. Heating the discotic dimers in cyclohexane and subsequently slow cooling down to room temperature yielded room temperature organic gels for the dimeric **Tp^{6}Th$_2$Tp^6**, **Tp^{6}Fu$_2$Tp^6**, **Tp^{8}Ph$_2$Tp^8**, **Tp^{8}TtTp^8** and **Tp^{8}BtTp^8**, with low critical (minimum) concentrations of 2–5 mg mL^{-1} (below 1%, they are termed supergelators), though the solutions

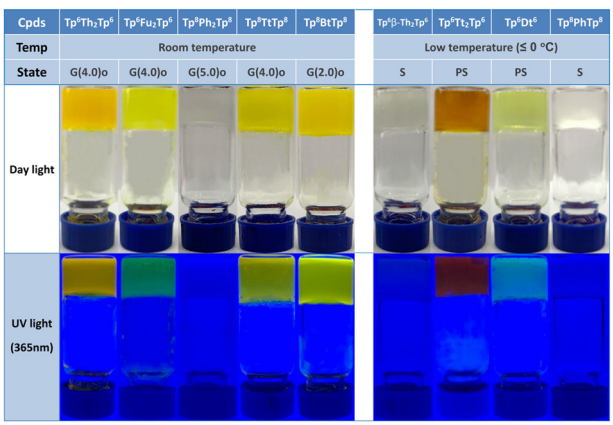

Fig. 10 Gels and frozen solutions of the dimers formed in cyclohexane on slow cooling, at room temperature and below 0 °C, in day light (top) and under UV irradiation (365 nm, bottom). G, S and PS indicate the state of the mixture corresponding to gel, solution and poor solution, respectively. The numbers in brackets correspond to the critical (minimum) gelation concentration (CGC/MGC) in mg mL^{-1}; "o" indicates that the gel is opaque.

started to gel at various temperatures on cooling. The other tested discotic dimers, *i.e.*, **Tp^{6}β-Th$_2$Tp^6**, **Tp^{6}Tt$_2$Tp^6**, **Tp^{6}Dt^6** and **Tp^{8}PhTp^8**, only form organo-gels when cooled down below 0 °C (Fig. S53, ESI†). Discotic dimers with short chains, **Tp^{6}Ph$_2$Tp^6**, **Tp^{6}TtTp^6** and **Tp^{6}BtTp^6**, exhibit inferior gelling behavior and show a tendency to crystallize from the solvents.

To gain some insights into the self-assembled gel microstructures or crystalline aggregation from solvents, xerogels/crystalline fibers, the re-precipitated micro-particles were studied by scanning electron microscopy, and the morphologies of the xerogels are shown in Fig. 11 and Fig. S54 (ESI†).

As revealed by SEM, the thiophene-bridged/fused discotic dimers (**Tp^{6}Th$_2$Tp^6**, **Tp^{6}Tt$_2$Tp^6**, **Tp^{6}Dt^6**, **Tp^{6,8}TtTp^{6,8}** and **Tp^{6,8}BtTp^{6,8}**) self-assemble into ultra-long net-shaped microwires with regular widths, demonstrating the balance of strong π–π core aggregations and the solubility of soft peripheral alkyl chains for these rigid discotic dimers. The gel formed from isomer **Tp^{6}β-Th$_2$Tp^6** shows a different morphology to that of **Tp^{6}Th$_2$Tp^6**, assembling into rigid micro-plates with about 100 μm length and 10 μm width; this morphology further reflects the fact that **Tp^{6}β-Th$_2$Tp^6** has a rigid, twisted backbone and limited free-rotation conformation. The bifuran-bridged dimer **Tp^{6}Fu$_2$Tp^6**, having a good solubility in most organic solvents but weaker π–π stacking interactions, did not form regular micro fibers. **Tp^{6,8}PhTp^{6,8}** and **Tp^{6,8}Ph$_2$Tp^{6,8}**, with a phenyl and biphenyl bridge, respectively, assemble into irregular micro particles. The SEM results here reveal the advantages of thiophene-containing building blocks for ordered self-assembling architectures. Compared with the fused π-conjugated polycyclic aromatic hydrocarbons (PAH) recently reported,[34–36] these original discotic dimers show weaker gelling ability of organic solvent, due to the higher rotational freedom of both discogenic TPs and weaker π–π stacking interactions with the molecules of solvent. In polar organic solvents and aromatic hydrocarbon solvents, they show good solubility and organogels were not formed. Furthermore, the shorter-chain discotic dimers had better solubility in organic solvent and lower gelling ability. However, the discotic dimers with longer peripheral chains formed gels in cyclohexane.

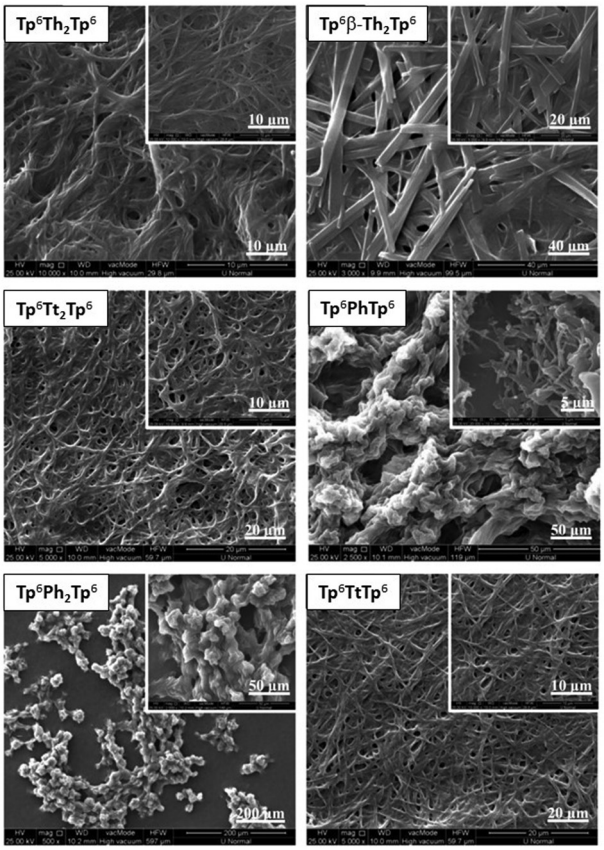

Fig. 11 Self-assembled morphologies of some representative π-bridged dimers: SEM images of xerogels or solution-deposited micro-particles from organic solvents.

Conclusions

Triphenylene nonaflates were used in Suzuki–Miyaura cross-coupling reactions for large scale synthesis of aryl-triphenylene and triphenylene discotic dimers. Bifuran-, bithiophene- and bithienothiophene-bridged dimers were synthesized by $FeCl_3$ oxidative homo-coupling dimerization from the corresponding thiophene-, furan-, and thienothiophene-triphenylene. Moreover, $FeCl_3$ oxidative cross-coupling of 2-thiophene- and 2-thieno[3,2-*b*]thiophene-triphenylene with electron-rich 3,3′,4,4′-tetra(alkoxy)-biphenyl (annulated π-extension, APEX) afforded two original, unsymmetrical thiophene-fused dimers, the latter prepared in quite a good yield.

All discotic dimers exhibited columnar (rectangular, hexagonal, and nematic) mesophases, over broad temperature ranges. From the SWAXS data and geometrical analysis, and supported by direct STM imaging, the col_{rec} mesophase organization is thought to result from the disposition of 6 dimers into a chevron arrangement, whereas the formation of the hexagonal columnar mesophases necessarily results from the exact positioning of every triphenylene moieties (half a dimer) at the nodes of a hexagonal network (to yield single TP columns), with in-plane translational and/or orientational disorder. The nematic columnar phase results from short-range stacked twinned-columns, with a long-range axial order.

These rigid discotic dimers also show strong fluorescence in solution and in thin films, with emission color, ranging from blue to red, depending on the bridge π-conjugation length and the overall molecular conformation; therefore, they represent an original set of full-color tunable photoluminescent liquid crystalline materials. Furthermore, most of the dimers show moderate to high fluorescence quantum yields (Φ) in solution, and, in particular, the bifuran-bridged dimer shows the highest Φ value near 66.3%. These experimental measurements were fully supported by theoretical DFT computing calculation.

These dimeric compounds also form gels in cyclohexane and emit blue-to-orange light when irradiated by UV light. SEM revealed that their gelation ability results from the entanglements of, depending on the bridge and chain lengths, ultra-long or thin microfibers into intricate 3D morphologies.

The facile synthesis of these exclusive, potentially multifunctional rigid discotic dimers, their rich mesomorphism, strong gelation ability and fine-tuned photophysical properties make these materials very attractive in the active field of organic electronics. This methodology could be applicable to many other discotic and bridge system combinations (symmetrical and non-symmetrical), with the additional possibility to modify the nature of the terminal flexible chains in order to tame the electronic and organizational properties.

Author contributions

The manuscript was written through contributions of all authors. All authors have given approval to the final version of the manuscript.

Conflicts of interest

There are no conflicts to declare.

Acknowledgements

This work was financially supported by the National Natural Science Foundation of China (Contract No. 21772135, 51773140, and 51973143). BD thanks the CNRS and the University of Strasbourg for support.

Notes and references

1 T. Kato, M. Yoshio, T. Ichikawa, B. Soberats, H. Ohno and M. Funahashi, *Nat. Rev. Mater.*, 2017, **2**, 17001.
2 A. C. Grimsdale and K. Müllen, *Angew. Chem., Int. Ed.*, 2005, **44**, 5592–5629.
3 R. E. Martin and F. Diederich, *Angew. Chem., Int. Ed.*, 1999, **38**, 1350–1377.
4 A. Suzuki, *Angew. Chem., Int. Ed.*, 2011, **50**, 6722–6737.
5 A. A. O. Sarhan and C. Bolm, *Chem. Soc. Rev.*, 2009, **38**, 2730–2744.
6 Y. D. Yang, J. B. Lan and J. S. You, *Chem. Rev.*, 2017, **117**, 8787–8863.
7 T. Doba, L. Ilies, W. Sato, R. Shang and E. Nakamura, *Nat. Catalysis*, 2021, **4**, 631–638.
8 M. Grzybowski, B. Sadowski and H. Butenschön, *Angew. Chem., Int. Ed.*, 2020, **59**, 2998–3027.
9 K. Q. Zhao, J. Q. Du, X. H. Long, M. Jing, B. Q. Wang, P. Hu, H. Monobe, B. Henrich and B. Donnio, *Dyes Pigm.*, 2017, **143**, 252–260.
10 K. Q. Zhao, M. Jing, L. L. An, J. Q. Du, Y. H. Wang, P. Hu, B. Q. Wang, H. Monobe, B. Heinrich and B. Donnio, *J. Mater. Chem. C*, 2017, **5**, 669–682.
11 D. Myśliwiec, B. Donnio, P. J. Chmielewski, B. Heinrich and M. Stępień, *J. Am. Chem. Soc.*, 2012, **134**, 4822–4833.
12 R. J. Bushby, S. M. Kelly and M. O'Neill, *Liquid Crystalline Semiconductors*, Springer, 2013.
13 R. J. Bushby and O. R. Lozman, *Curr. Opin. Colloid Interface Sci.*, 2002, **7**, 343–354.
14 R. J. Bushby and O. R. Lozman, *Curr. Opin. Solid State Mater. Sci.*, 2002, **6**, 569–578.
15 S. Chandrasekhar, B. K. Sadashiva and K. A. Suresh, *Pramana*, 1977, **9**, 471–480.
16 T. Wöhrle, I. Wurzbach, J. Kirres, A. Kostidou, N. Kapernaum, J. Litterscheidt, J. C. Haenle, P. Staffeld, A. Baro, F. Giesselmann and S. Laschat, *Chem. Rev.*, 2016, **116**, 1139–1241.
17 S. Sergeyev, W. Pisula and Y. H. Geerts, *Chem. Soc. Rev.*, 2007, **36**, 1902–1929.
18 F. J. M. Hoeben, P. Jonkheijm, E. W. Meijer and A. P. H. J. Schenning, *Chem. Rev.*, 2005, **105**, 1491–1546.
19 M. Lehmann, S. Gloza and S. Roth, *Chem. Mater.*, 2015, **27**, 8181–8184.
20 S. Park and B. K. Cho, *Soft Matter*, 2015, **11**, 94–101.
21 E. Beltrán, J. Barberá, J. L. Serrano, A. Elduque and R. Giménez, *Eur. J. Inorg. Chem.*, 2014, 1165–1173.
22 M. Masuda, M. Kohri and K. Kishikawa, *Liq. Cryst.*, 2021, **48**, 295–306.
23 M. A. Shcherbina, X. B. Zeng, T. Tadjiev, G. Ungar, S. H. Eichhorn, K. E. S. Phillips and T. J. Katz, *Angew. Chem., Int. Ed.*, 2009, **48**, 7837–7840.
24 Y. Cao, M. Alaasar, L. Zhang, C. H. Zhu, C. Tschierske and F. Liu, *J. Am. Chem. Soc.*, 2022, **144**, 6936–6945.
25 S. H. Eichhorn, A. O. El-Ballouli, A. Cassar and B. R. Kaafarani, *ChemPlusChem*, 2021, **86**, 319–339.
26 M. Lehmann, M. Dechant, M. Lambov and T. Ghosh, *Acc. Chem. Res.*, 2019, **52**, 1653–1664.
27 M. Dechant, M. Lehmann, G. Uzurano, A. Fujii and M. Ozaki, *J. Mater. Chem. C*, 2021, **9**, 5689–5698.
28 T. Ghosh, L. Gerbig, M. Lambov, M. Dechant and M. Lehmann, *J. Mater. Chem. C*, 2020, **8**, 5562–5571.
29 M. Hügel, M. Dechant, N. Scheuring, T. Ghosh and M. Lehmann, *Chem. – Eur. J.*, 2019, **25**, 3352–3361.
30 M. Lehmann, *Top. Curr. Chem.*, 2012, **318**, 193–224.
31 N. Tober, J. Winter, M. Jochem, M. Lehmann and H. Detert, *Eur. J. Org. Chem.*, 2021, 798–809.
32 H. Taing, A. M. Cassar, M. U. Ocheje, S. Rondeau-Gagné, T. H. El-Assaad, C. A. Sharabati, B. R. Kaafarani and S. H. Eichhorn, *ChemPlusChem*, 2019, **84**, 103–106.
33 X. M. Zhu, X. Y. Bai, H. F. Wang, P. Hu, B. Q. Wang and K. Q. Zhao, *Acta Chim. Sin.*, 2021, **79**, 1486–1493.
34 T. Ma, H. F. Wang, K. Q. Zhao, B. Q. Wang, P. Hu, H. Monobe, B. Heinrich and B. Donnio, *ChemPlusChem*, 2019, **84**, 1439–1448.
35 T. Ma, Y. J. Zhong, H. F. Wang, K. Q. Zhao, B. Q. Wang, P. Hu, H. Monobe and B. Donnio, *Chem. – Asian J.*, 2021, **16**, 1106–1117.
36 J. F. Hang, H. Lin, K. Q. Zhao, P. Hu, B. Q. Wang, H. Monobe, C. H. Zhu and B. Donnio, *Eur. J. Org. Chem.*, 2021, 1989–2002.
37 F. Lincker, A. J. Attias, F. Mathevet, B. Heinrich, B. Donnio, J. L. Fave, P. Rannou and R. Demadrille, *Chem. Commun.*, 2012, **48**, 3209–3211.

38 F. Lincker, B. Heinrich, R. D. Bettignies, P. Rannou, J. Pécaut, B. Grévin, A. Pron, B. Donnio and R. Demadrille, *J. Mater. Chem.*, 2011, **21**, 5238–5247.
39 C. X. Liu, H. Wang, J. Q. Du, K. Q. Zhao, P. Hu, B. Q. Wang, H. Monobe, B. Heinrich and B. Donnio, *J. Mater. Chem. C*, 2018, **6**, 4471–4478.
40 O. Kwon, X. Q. Cai, W. T. Qu, F. Liu, J. Szydłowska, E. Gorecka, M. J. Han, D. K. Yoon, S. Poppe and C. Tschierske, *Adv. Funct. Mater.*, 2021, **31**, 2102271.
41 T. Yasuda, T. Shimizu, F. Liu, G. Ungar and T. Kato, *J. Am. Chem. Soc.*, 2011, **133**, 13437–13444.
42 Y. F. Li, A. Concellon, C. J. Lin, N. A. Romero, S. B. Lin and T. M. Swager, *Chem. Sci.*, 2020, **11**, 4695–4701.
43 Q. Xiao, T. Sakurai, T. Fukino, K. Akaike, Y. Honsho, A. Saeki, S. Seki, K. Kato, M. Takata and T. Aida, *J. Am. Chem. Soc.*, 2013, **135**, 18268–18271.
44 I. Bala, J. De, S. P. Gupta, H. Singh, U. K. Pandey and S. K. Pal, *Chem. Commun.*, 2020, **56**, 5629–5632.
45 L. X. Guo, Y. B. Xing, M. Wang, Y. Sun, X. Q. Zhang, B. P. Lin and H. Yang, *J. Mater. Chem. C*, 2019, **7**, 4828–4837.
46 N. Hu, R. F. Shao, Y. Q. Shen, D. Chen, N. A. Clark and D. M. Walba, *Adv. Mater.*, 2014, **26**, 2066–2071.
47 A. Demenev, S. H. Eichhorn, T. Taerum, D. F. Perepichka, S. Patwardhan, F. C. Grozema, L. D. A. Siebbeles and R. Klenkler, *Chem. Mater.*, 2010, **22**, 1420–1428.
48 D. M. Knawby and T. M. Swager, *Chem. Mater.*, 1997, **9**, 535–538.
49 K. C. Zhao, J. Q. Du, H. F. Wang, K. Q. Zhao, P. Hu, B. Q. Wang, H. Monobe, B. Heinrich and B. Donnio, *Chem. – Asian J.*, 2019, **14**, 462–470.
50 W. J. Deng, S. Liu, H. Lin, K. X. Zhao, X. Y. Bai, K. Q. Zhao, P. Hu, B. Q. Wang, H. Monobe and B. Donnio, *New J. Chem.*, 2022, **46**, 7936–7949.
51 S. Kumar, *Liq. Cryst.*, 2005, **32**, 1089–1113.
52 S. Kumar and S. K. Varshney, *Liq. Cryst.*, 2001, **28**, 161–163.
53 S. Kumar and S. K. Varshney, *Org. Lett.*, 2002, **4**, 157–159.
54 K. Q. Zhao, H. Zhou, W. H. Yu, B. Q. Wang and P. Hu, *Acta Chim. Sin.*, 2011, **69**, 1895–1902.
55 Y. Yang, H. Wang, H. F. Wang, C. X. Liu, K. Q. Zhao, B. Q. Wang, P. Hu, H. Monobe, B. Heinrich and B. Donnio, *Cryst. Growth Des.*, 2018, **18**, 4296–4305.
56 L. Zhang, H. Gopee, D. L. Hughes and A. N. Cammidge, *Chem. Commun.*, 2010, **46**, 4255–4257.
57 L. Zhang, D. L. Hughes and A. N. Cammidge, *J. Org. Chem.*, 2012, **77**, 4288–4297.
58 W. K. Xiao, Z. Q. He, S. Remiro-Buenamañana, R. J. Turner, M. Xu, X. Yang, X. P. Jing and A. N. Cammidge, *Org. Lett.*, 2015, **17**, 3286–3289.
59 H. Ito, K. Ozaki and K. Itami, *Angew. Chem., Int. Ed.*, 2017, **56**, 11144–11164.
60 H. Ito, Y. Segawa, K. Murakami and K. Itami, *J. Am. Chem. Soc.*, 2019, **141**, 3–10.
61 S. Kumar, *Liq. Cryst.*, 2004, **31**, 1037–1059.
62 S. Kumar and J. J. Naidu, *Liq. Cryst.*, 2002, **29**, 899–906.
63 D. Adam, P. Schuhmacher, J. Simmerer, L. Häussling, K. Siemensmeyer, K. H. Etzbach, H. Ringsdorf and D. Haarer, *Nature*, 1994, **371**, 141–143.
64 R. J. Bushby and K. Kawata, *Liq. Cryst.*, 2011, **38**, 1415–1426.
65 R. Chico, C. Domínguez, B. Donnio, B. Heinrich, S. Coco and P. Espinet, *Cryst. Growth Des.*, 2016, **16**, 6984–6991.
66 R. Chico, E. de Domingo, C. Domínguez, B. Donnio, B. Heinrich, R. Termine, A. Golemme, S. Coco and P. Espinet, *Chem. Mater.*, 2017, **29**, 7587–7595.
67 A. B. Miguel-Coello, M. Bardají, S. Coco, B. Donnio, B. Heinrich and P. Espinet, *Inorg. Chem.*, 2018, **57**, 4359–4369.
68 D. Zeng, I. Tahar-Djebbar, Y. Xiao, F. Kameche, N. Kayunkid, M. Brinkmann, D. Guillon, B. Heinrich, B. Donnio, D. A. Ivanov, E. Lacaze, D. Kreher, F. Mathevet and A. Attias, *Macromol.*, 2014, **47**, 1715–1731.
69 A. Zelcer, B. Donnio, C. Bourgogne, F. D. Cukiernik and D. Guillon, *Chem. Mater.*, 2007, **19**, 1992–2006.
70 K. Q. Zhao, L. L. An, X. B. Zhang, W. H. Yu, P. Hu, B. Q. Wang, J. Xu, Q. D. Zeng, H. Monobe, Y. Shimizu, B. Heinrich and B. Donnio, *Chem. – Eur. J.*, 2015, **21**, 10379–10390.
71 K. Q. Zhao, X. Y. Bai, B. Xiao, Y. Gao, P. Hu, B. Q. Wang, Q. D. Zeng, C. Wang, B. Heinrich and B. Donnio, *J. Mater. Chem. C*, 2015, **3**, 11735–11746.
72 H. Lin, Q. B. Lv, H. F. Wang, K. Q. Zhao, P. Hu, B. Q. Wang, B. Heinrich and B. Donnio, *Dyes Pigm.*, 2022, **197**, 109911.
73 H. K. Bisoyi and S. Kumar, *Chem. Soc. Rev.*, 2010, **39**, 264–285.
74 S. Kumar and B. Lakshmi, *Tetrahedron Lett.*, 2005, **46**, 2603–2605.
75 K. Q. Zhao, Y. Gao, W. H. Yu, P. Hu, B. Q. Wang, B. Heinrich and B. Donnio, *Eur. J. Org. Chem.*, 2016, 2802–2814.
76 S. J. Mahoney, M. M. Ahmida, H. Kayal, N. Fox, Y. Shimizu and S. H. Eichhorn, *J. Mater. Chem.*, 2009, **19**, 9221–9232.
77 H. Bengs, O. Karthaus, H. Ringsdorf, C. Baehr, M. Ebert and J. H. Wendorff, *Liq. Cryst.*, 1991, **10**, 161–168.
78 N. Boden, R. C. Borner, R. J. Bushby, A. N. Cammidge and M. V. Jesudason, *Liq. Cryst.*, 1993, **15**, 851–858.
79 N. Boden, R. J. Bushby and A. N. Cammidge, *J. Am. Chem. Soc.*, 1995, **117**, 924–927.
80 C. F. Nising, U. K. Schmid, M. Nieger and S. Bräse, *J. Org. Chem.*, 2004, **69**, 6830–6833.
81 Y. Hirai, H. Monobe, N. Mizoshita, M. Moriyama, K. Hanabusa, Y. Shimizu and T. Kato, *Adv. Funct. Mater.*, 2008, **18**, 1668–1675.
82 B. Donnio, B. Heinrich, H. Allouchi, J. Kain, S. Dele, D. Guillon and D. W. Bruce, *J. Am. Chem. Soc.*, 2004, **126**, 15258–15268.
83 Y. L. Yang and C. Wang, *Chem. Soc. Rev.*, 2009, **38**, 2576–2589.
84 K. S. Mali, J. Adisoejoso, E. Ghijsens, I. de Cat and S. de Feyter, *Acc. Chem. Res.*, 2012, **45**, 1309–1320.
85 S. S. Babu, V. K. Praveen and A. Ajayaghosh, *Chem. Rev.*, 2014, **114**, 1973–2129.

